IBRO Reports 6 (2019) 1–17

Contents lists available at ScienceDirect

IBRO Reports

journal homepage: www.elsevier.com/locate/ibror

Research Paper

Layer-specific expression of extracellular matrix molecules in the mouse somatosensory and piriform cortices

Hiroshi Ueno[a,*], Shunsuke Suemitsu[b], Shinji Murakami[b], Naoya Kitamura[b], Kenta Wani[b], Yosuke Matsumoto[c], Motoi Okamoto[d], Takeshi Ishihara[b]

[a] Department of Medical Technology, Kawasaki University of Medical Welfare, 288, Matsushima, Kurashiki, Okayama, 701-0193, Japan
[b] Department of Psychiatry, Kawasaki Medical School, Kurashiki, 701-0192, Japan
[c] Department of Neuropsychiatry, Graduate School of Medicine, Dentistry and Pharmaceutical Sciences, Okayama University, Okayama, 700-8558, Japan
[d] Department of Medical Technology, Graduate School of Health Sciences, Okayama University, Okayama, 700-8558, Japan

ARTICLE INFO

Keywords:
Extracellular matrix
Perineuronal nets
Piriform cortex
Proteoglycans
Somatosensory cortex
Wisteria floribunda

ABSTRACT

In the developing central nervous system (CNS), extracellular matrix (ECM) molecules have regulating roles such as in brain development, neural-circuit maturation, and synaptic-function control. However, excluding the perineuronal net (PNN) area, the distribution, constituent elements, and expression level of granular ECM molecules (diffuse ECM) present in the mature CNS remain unclear. Diffuse ECM molecules in the CNS share the components of PNNs and are likely functional. As cortical functions are greatly region-dependent, we hypothesized that ECM molecules would differ in distribution, expression level, and components in a region- and layer-dependent manner. We examined the layer-specific expression of several chondroitin sulfate proteoglycans (aggrecan, neurocan, and brevican), tenascin-R, *Wisteria floribunda* agglutinin (WFA)-positive molecules, hyaluronic acid, and link protein in the somatosensory and piriform cortices of mature mice. Furthermore, we investigated expression changes in WFA-positive molecules due to aging. In the somatosensory cortex, PNN density was particularly high at layer 4 (L4), but not all diffuse ECM molecules were highly expressed at L4 compared to the other layers. There was almost no change in tenascin-R and hyaluronic acid in any somatosensory-cortex layer. Neurocan showed high expression in L1 of the somatosensory cortex. In the piriform cortex, many ECM molecules showed higher expression in L1 than in the other layers. However, hyaluronic acid showed high expression in deep layers. Here, we clarified that ECM molecules differ in constituent elements and expression in a region- and layer-dependent manner. Region-specific expression of ECM molecules is possibly related to functions such as region-specific plasticity and vulnerability.

Introduction

In the mature central nervous system (CNS), extracellular matrix (ECM) molecules are distributed as granular ECM molecules (diffuse ECM molecules) or concentrated meshwork structured perineuronal nets (PNNs) (Celio et al., 1998; Maeda, 2015). Generally, the ECM fills the extracellular region of all organs and tissues and contains water and ions (Mouw et al., 2014; Maeda, 2015). Unlike other organs, collagen fibers do not exist in the cortex of the brain, but instead contain many chondroitin sulfate proteoglycans (CSPGs). The ECM in the CNS is formed from hyaluronic acid, tenescin-R, glycoprotein, CSPG, and link protein (Maeda, 2015). Hyaluronic acid binds to CSPG via link protein. Tenascin-R combines with CSPGs. However, these relationships have been investigated only in the PNN area (the area the PNN occupies around the neuron) and the relationships of ECM molecules existing outside the PNN area remain unknown. The ECM molecules of the CNS regulate neuronal migration, axon outgrowth, synapse formation, and synapse maturation in the developmental phase (Curran and D'Arcangelo, 1998; Bandtlow and Zimmermann, 2000; Zimmermann and Dours-Zimmermann, 2008; Frischknecht and Gundelfinger, 2012).

Abbreviations: a.u., arbitrary units; ChABC, chondroitinase ABC; CNS, central nervous system; CSPG, chondroitin sulfate proteoglycans; ECM, extracellular cellular matrix; HABP, hyaluronic acid binding protein; HA, hyaluronic acid; Hapln1, hyaluronan and proteoglycan link protein 1; PNN, perineuronal ntes; WFA, Wisteria floribunda agglutinin

* Corresponding author.
E-mail addresses: dhe422007@s.okayama-u.ac.jp (H. Ueno), ssue@med.kawasaki-m.ac.jp (S. Suemitsu), muraka@med.kawasaki-m.ac.jp (S. Murakami), n-kitamura@med.kawasaki-m.ac.jp (N. Kitamura), k-wani@med.kawasaki-m.ac.jp (K. Wani), ymatsumoto@cc.okayama-u.ac.jp (Y. Matsumoto), mokamoto@md.okayama-u.ac.jp (M. Okamoto), t-ishihara@med.kawasaki-m.ac.jp (T. Ishihara).

https://doi.org/10.1016/j.ibror.2018.11.006
Received 29 September 2018; Accepted 24 November 2018

In the mature CNS, the function and distribution of ECM molecules existing outside the PNN area have not been clarified.

In the CNS, there is PNN in the structure where ECM molecules are condensed. The PNN is a reticular structure surrounding the neuronal soma, axon initial segment, and proximal dendrites of particular neurons (Slaker et al., 2016). In the cortex and hippocampus, the PNN is mainly formed around parvalbumin-positive GABAergic interneurons (Slaker et al., 2016). The PNN maintains the cellular ion homeostasis of highly active neurons (Brückner et al., 1993; Härtig et al., 1999), stabilizes synaptic connections, and regulates synaptic plasticity (Kalb and Hockfield, 1994; Pizzorusso et al., 2002). The PNN is formed in the late phase of the developmental period and is considered to control the critical period of brain development because it is related to the end of synaptic plasticity. Depending on the constituent CSPG, the PNN hinders the formation of new synaptic connections by inhibiting axonal sprouting (McKeon et al., 1995; Smith-Thomas et al., 1995; Zuo et al., 1998). Therefore, it has been reported that synaptic plasticity of the mature visual cortex is restored by denaturing CSPG on PNNs with chondroitinase ABC injection (ChABC) (Pizzorusso et al., 2002; Berardi et al., 2004). In addition, PNNs protect the surrounding neurons from oxidative stress and glutamate-stimulated excitotoxicity (Okamoto et al., 1994; Morawski et al., 2004).

On the other hand, the PNN is frequently expressed in the spinal cord (Jäger et al., 2013). However, it is considered that it is not the PNN itself but ECM molecules that inhibit axonalits axon outgrowth (Gaudet and Popovich, 2014). Even in the cortex and hippocampus, parvalbumin-positive neurons surrounded by PNNs alone are not responsible for neuroplasticity preservation and protective function, but there is a high possibility that ECM molecules dispersed in granular form also have similar functions.

Changes in ECM molecules have been reported in the brains of patients with Alzheimer's disease (AD) and schizophrenia (Bonneh-Barkay and Wiley, 2009; Pantazopoulos et al., 2010). However, the related cause and mechanism remain unknown. Reportedly, ECM molecules are implicated in the etiology of AD (Brückner et al., 1999), and it has been suggested that ECM structure has a neuroprotective function in AD (Morawski et al., 2010). It has been reported that PNN protects neurons from amyloid beta toxicity and oxidative stress (Miyata et al., 2007; Suttkus et al., 2014). Neurons surrounded by PNNs are less prone to neurofibrillary tangles in AD. In patients with AD or schizophrenia, disorders only occur in specific brain regions and they may be due to brain region-specific ECM molecule expression. Changes in ECM molecules in several diseases have been investigated, but the differences among ECM components and expression levels in normal brain regions and each layer remain unclear.

Quantitative analysis of ECM molecules in each brain region and each layer has not been performed, which is important to elucidate the role of ECM molecules in normal and pathological conditions. In this study, we mainly examined the diffuse ECM molecules. We examined the layer-specific expression of several CSPGs (aggrecan, neurocan, and brevican), tenascin-R, WFA-positive molecules, hyaluronic acid, and link protein (cartilage link protein 1 (Crtl1/Hapln1)) in the somatosensory and piriform cortices of mature mice. Furthermore, changes in WFA-positive molecules in these cortices due to aging were analyzed. WFA binds to N-acetylgalactosamine, terminal ends of CSPGs (Nakagawa et al., 1986; Härtig et al., 1992; Brückner et al., 1993; Schweizer et al., 1993; Seeger et al., 1994). AB1031 used to label aggrecan recognizes the central protein domain in the chondroitin sulfate glycosaminoglycan binding region of aggrecan (Giamanco et al., 2010; Lendvai et al., 2013). Cat-315 is an antibody recognizing HNK-1 carbohydrate epitope of aggrecan (Matthews et al., 2002; Dino et al., 2006; McRae et al., 2007). Revealing the distribution of ECM molecules would contribute to the elucidation of these functions in neurodegenerative and neuropsychological diseases.

Experimental procedures

Animals

Male mice (C57BL/6 N) were used for experiments. We used male mice for these studies in order to eliminate the effects of the estrous cycle in females. The mice were divided into six groups according to age: postnatal week 2 (2 w; n = 5), 3 w (n = 5), 4 w (n = 5), 11 w (n = 5), 1 years old (1y; n = 5), and 2y (n = 5). Mice were housed five to a cage under standard laboratory conditions. All procedures related to animal maintenance and experimentation were approved by the Committee for Animal Experiments at Kawasaki Medical School Advanced Research Center and conformed to the U.S. National Institutes of Health (NIH) Guide for the Care and Use of Laboratory Animals (NIH Publication No. 80-23, revised in 1996). We purchased the mice from Charles River Laboratories (Kanagawa, Japan). The mice were housed in cages including the provision of nesting material with food and water provided ad libitum, under light/dark conditions (lights on at 7:00 A.M., lights off at 9:00 P.M.) and temperature maintained at 23–26 °C.

Tissue preparation

Mice were anesthetized with a lethal dose of sodium pentobarbital (120 mg/kg, i.p.) and transcardially perfused with 25 mL of phosphate-buffered saline (PBS) followed by 100 mL of 4% paraformaldehyde in PBS (pH 7.4). Brains were dissected and post-fixed overnight at 4 °C in the above fixative. The brains were then cryoprotected in 15% sucrose for 12 h followed by 30% sucrose for 20 h at 4 °C. Next, the brains were frozen in an optimum cutting temperature compound (Tissue-Tek; Sakura Finetek, Tokyo, Japan) using a slurry of normal hexane in dry ice. Serial coronal sections with a thickness of 40-μm were obtained at −20 °C using a cryostat (CM3050S; Leica Wetzlar, Germany). The sections were collected in ice-cold PBS containing 0.05% sodium azide.

Immunohistochemistry

We treated the cryostat sections with 0.1% Triton X-100 with PBS at room temperature for 15 min. After three washes with PBS, we incubated the sections with 10% normal goat serum (ImmunoBioScience Corp., Mukilteo, WA) in PBS at room temperature for 1 h, we washed them three times with PBS, and incubated them overnight at 4 °C in PBS containing biotinylated WFA (B-1355, Vector Laboratories; 1:200) and the antibodies described in the subsection Antibodies and Lectins. After washing with PBS, we incubated the sections with the corresponding secondary antibodies (described in the subsection Antibodies and lectins) and Alexa Fluor 594-conjugated streptavidin (S11227; Molecular Probes, Eugene, OR) at room temperature for 2 h. We rinsed the labeled sections again with PBS and we mounted them on glass slides with Vectashield medium (H-1400; Vector Laboratories, Funakoshi Co., Tokyo, Japan). We stored the prepared slides at 4 °C until we used them in the microscopy analysis.

Antibodies and lectins

We used the following lectins and primary antibodies for staining: biotinylated WFA (B-1355, Vector Laboratories; 1:200), biotinylated HABP (385911; MERCK; 1:200), goat anti-Crtl1/Hapln1 (AF260, R&D Systems, Minneapolis, MN, USA; 1:50), goat anti-tenascin-R (AF3865, R &D Systems; 1:200), rabbit anti-aggrecan (AB1031, MERCK; 1:200), sheep anti-neurocan (AF5800, R&D Systems, 1:25), sheep anti-brevican (AF4009, R&D Systems, 1:200), mouse anti-aggrecan (Cat-315; MAB1581, MERCK; 1:1000), mouse anti-GAD67 (clone 1G10.2, MAB5406; Millipore, Bedford, MA; 1:1,000), and guinea pig anti-VGLUT1 (AB5905; Millipore; 1:1,000) (Table 1).

We used the following secondary antibodies for visualization: Alexa

Table 1
Primary antibodies used in this study.

Primary antibody	Immunogen	Manufacture (catalog No.)	Host species	Dilution used
Hapln1	E. coli-derived recombinant human CXCL11/I-TAC	R&D Systems, Minneapolis, MN, USA (AF260)	goat polyclonal	1:50
Tenascin-R	Mouse myeloma cell line NS0-derived recombinant human Tenascin R isoform 1	R&D Systems, Minneapolis, MN, USA (AF3865)	goat polyclonal	1:200
AB1031	GST fusion protein containing amino acids 1177-1326 of mouse aggrecan	Millipore, Billerica, MA, USA (AB1031)	rabbit polyclonal	1:200
Neurocan	Chinese hamster ovary cell line CHO-derived recombinant mouse Neurocan	R&D Systems, Minneapolis, MN, USA (AF5800)	sheep polyclonal	1:25
Brevican	Mouse myeloma cell line NS0-derived recombinant human Brevican	R&D Systems, Minneapolis, MN, USA (AF4009)	sheep polyclonal	1:200
Cat-315	Feline brain proteoglycans	Millipore, Billerica, MA, USA (MAB1581)	mouse monoclonal	1:1000
GAD67	Recombinant GAD67 protein	Millipore, Billerica, MA, USA (MAB5406)	mouse monoclonal	1:1000
VGLUT1	Synthetic peptide from rat VGLUT1 protein with no overlap to VGLUT2	Millipore, Billerica, MA, USA (AB5905)	guinea pig polyclonal	1:100

Fluor 488-conjugated goat anti-mouse IgG (ab150113; Abcam, Cambridge, MA; 1:1,000), Alexa Fluor 594-conjugated goat anti-guinea pig (A-11076; Thermo Fisher Scientific, Waltham, MA; 1:500), FITC-conjugated anti-mouse IgM (sc-2082, Santa Cruz Biotechnology, Santa Cruz, CA, 1:1000), Alexa Fluor 488-conjugated goat anti-rabbit IgG (ab150077, Abcam; 1:1000), DyLight 488-conjugated horse anti-goat IgG (DI-3088; Vector Laboratories; 1:500), Alexa Fluor 488-conjugated donkey anti-sheep IgG (A-11015; Thermo Fisher Scientific, 1:500), and streptavidin-conjugated Alexa Fluor 594 (S11227, Thermo Fisher Scientific; 1:1000).

Microscopy imaging

For quantification of the density of WFA-positive PNNs and analysis of ECM fluorescence intensities, we used confocal laser scanning microscopy (LSM700; Carl Zeiss, Oberkochen, Germany) to obtain images of stained sections. Images (1024 × 1024 pixels) were saved as TIFF files using the ZEN software (Carl Zeiss). Briefly, we performed the analysis using a 10× objective lens and a pinhole setting that corresponded to a focal plane thickness of less than 1 μm. For observing ECM molecules, GAD67- and VGLUT1-positive synaptic terminals, samples were randomly selected and high-magnification images using a 100× objective lens were acquired. Prior to capture, the exposure time, gain, and offset were carefully set to ensure a strong signal but to avoid saturation. Identical capture conditions were used for all sections. Images from whole sections were acquired using a 10× objective lens of a fluorescence microscope (BZ-X; KEYENCE, Tokyo, Japan) and we merged them using the KEYENCE BZ-X Analyzer software (KEYENCE).

Quantification of labeled PNNs and ECMs

Brain areas were determined according to the atlas by Paxinos and Franklin (2012). Data shown in the figures are presented according to the cortical layer profiles based on fluorescence Nissl staining (NeuroTrace 435/455 blue: N-21479, Molecular Probes). We stored all confocal images as TIFF files and analyzed them using the NIH ImageJ software (Bethesda, MD; http://rsb.info.nih.gov/nih-image/). From each mouse, four coronal sections containing somatosensory cortex and piriform cortex (from -0.8 mm to -1.8 mm relative to bregma) were selected and processed for staining. We manually tagged stained PNNs (soma size larger than 60 μm^2) in the region of interest and counted them. PNN density was calculated as cells/mm^2. Quantifications were performed by a blinded independent observer. For quantifying the fluorescence intensity of ECM-positive molecules and WFA-positive PNNs, we selected four sections from each mouse brain and stained them as described above. The ellipse circumscribing the WFA-positive PNNs was traced manually on 8-bit images of each section, and the gray levels for WFA labeling were measured using the ImageJ software, which was assigned arbitrary units (a.u.). We manually outlined the parts excluding PNNs and measured the gray level with NIH ImageJ. Background intensity was subtracted using unstained portions of each section. We acquired all confocal images as TIFF files and analyzed them with NIH ImageJ. We coded the slides and a blinded independent observer quantified them.

Data analysis

Data are expressed as box plots of five animals per group. Statistical significance was determined by two-way analysis of variance followed by the Bonferroni t-tests. The statistical significance threshold was set at $p < 0.05$.

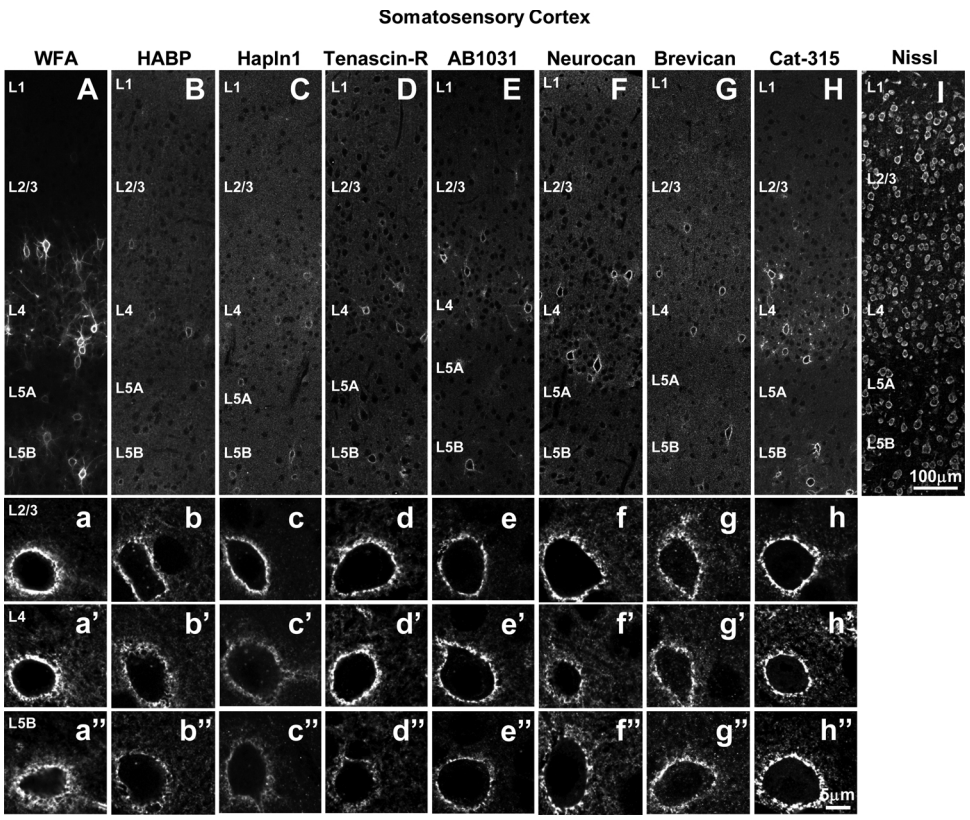

Fig. 1. Extracellular matrix molecules in the mouse somatosensory cortex.
Representative images show the laminar distribution of WFA-positive molecules (A), HABP-positive molecules (B), Hapln1-positive molecules (C), tenascin-R-positive molecules (D), AB1031-positive molecules (E), neurocan-positive molecules (F), brevican-positive molecules (G), Cat-315-positive molecules (H), and Nissl-positive cells (I) in the somatosensory cortex. High-magnification confocal images of WFA (a, a', a''), HABP (b, b', b''), Hapln1 (c, c', c''), tenascin-R (d, d', d''), AB1031 (e, e', e''), neurocan (f, f', f''), brevican (g, g', g''), and Cat-315 (h, h', h'') labeling in L2/3 (a–h), L4 (a'–h'), and L5B (a''–h'') of the mouse somatosensory cortex at postnatal week 11. Scale bars: 100 μm in I (applies to A–I); 5 μm in h'' (applies to a–h, a'–h', a''–h'').

Results

Extracellular matrix molecules in the mouse somatosensory cortex

To examine the spatial distribution of ECM molecules, we stained for WFA, HABP, Hapln1, tenascin-R, AB1031, neurocan, brevican, and Cat-315. ECM molecules were expressed in the neuropil of the mouse somatosensory and piriform cortices at 11 w (Figs. 1 and 2). Their distribution pattern was region-specific and layer-specific (Figs. 1A–H, and 2 A–H). In the somatosensory cortex, the highest level of ECM molecule expression was observed in layer 4 (L4) (Fig. 1A–H). In the piriform cortex, the highest level of ECM molecule expression was observed in the upper level of L1 (L1A) (Fig. 2A–H). High magnification showed that ECM molecules in granular form were scattered throughout the cortical layers of the mouse somatosensory and piriform cortices (Figs. 1a–h, a'–h', a''–h'', 2 a–h). In addition, ECM molecules revealed a characteristic pattern of PNN formation in the mouse somatosensory cortex (Fig. 1a–h, a'–h', a''–h'').

Comparative distribution of ECM molecules in the mouse somatosensory and piriform cortices

To examine whether ECM molecules may differ per cortical layer, we quantified layer-specific WFA, HABP, Hapln1, tenascin-R, AB1031,

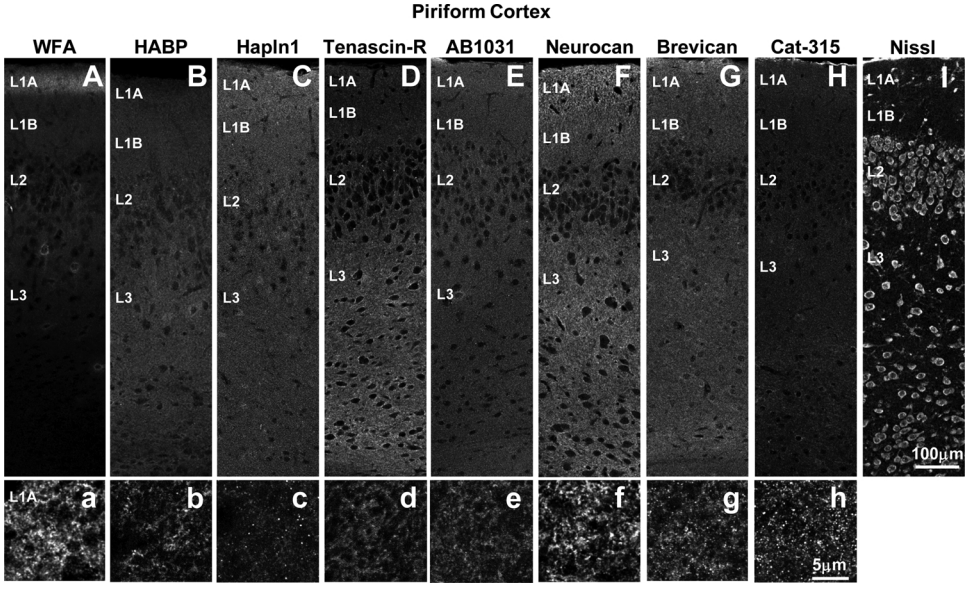

Fig. 2. Extracellular matrix molecules in the mouse piriform cortex.
Representative images show the laminar distribution of WFA-positive molecules (A), HABP-positive molecules (B), Hapln1-positive molecules (C), tenascin-R-positive molecules (D), AB1031-positive molecules (E), neurocan-positive molecules (F), brevican-positive molecules (G), Cat-315-positive molecules (H) and Nissl-positive cells (I) in the mouse piriform cortex at postnatal week 11. High-magnification confocal images of WFA (a), HABP (b), Hapln1 (c), tenascin-R (d), AB1031 (e), neurocan (f), brevican (g), and Cat-315 (h) labeling in L1A (a–h) of the mouse piriform cortex at postnatal week 11. Scale bars: 100 μm in I (applies to A–I); 5 μm in h (applies to a–h).

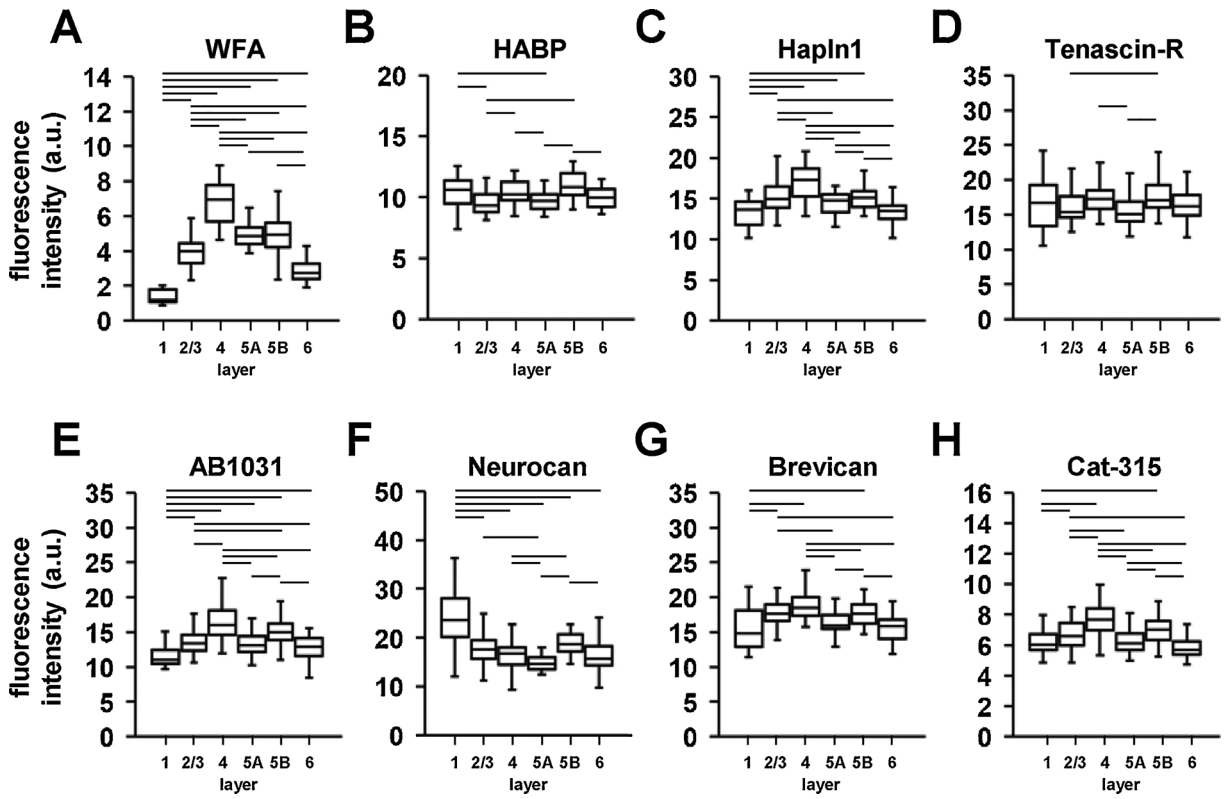

Fig. 3. Quantitative analyses of extracellular matrix molecules in the mouse somatosensory cortex.
Quantified mean fluorescence intensity of WFA-positive molecules (A), HABP-positive molecules (B), Hapln1-positive molecules (C), tenascin-R-positive molecules (D), AB1031-positive molecules (E), neurocan-positive molecules (F), brevican-positive molecules (G), and Cat-315-positive molecules (H), excluding the PNN, in the mouse somatosensory cortex at postnatal week 11. Data are expressed as box plots. *p < 0.05 for comparison between layers. The respective p values are listed in Table 2.
WFA: $F_{(5,269)} = 196.641$ in.(A). $p < 0.001$, HABP: $F_{(5,143)} = 6.772$, $p < 0.001$ in.(B), Hapln1: $F_{(5,269)} = 35.132$, $p < 0.001$ in.(C), tenascin-R: $F_{(5,269)} = 2.986$, $p = 0.012$ in.(D), AB1031: $F_{(5,228)} = 32.250$, $p < 0.001$ in.(E), neurocan: $F_{(5,269)} = 36.797$, $p < 0.001$ in.(F). brevican: $F_{(5,228)} = 16.721$, $p < 0.001$ in.(G), Cat-315: $F_{(5,251)} = 23.139$, $p < 0.001$ in.(H).

neurocan, brevican, and Cat-315-positive signal intensity, excluding the PNN area, in the mouse somatosensory cortex at 11 w (Fig. 3A–H, Table 2A), and mouse piriform cortex at 11 w (Fig. 4A–H, Table 2B). The fluorescence intensities of these ECM molecules were layer-specific.

In the mouse somatosensory cortex, the fluorescence intensity of ECM molecules showed significant variation among the layers. WFA-positive fluorescence intensity in L4 was very high compared with that in the other layers (Fig. 3A, Table 2A). WFA-positive fluorescence intensity in L1 was very low compared with that in the other layers. There was minor difference in the expression of HABP-positive molecules among the layers (Fig. 3B, Table 2A). Hapln1-positive fluorescence intensity in L4 was very high compared with that in the other layers (Fig. 3C, Table 2A). There was minor difference in the expression of tenascin-R-positive fluorescence intensity between the layers (Fig. 3D, Table 2A). AB1031-positive fluorescence intensity in L4 was very high compared with that in the other layers (Fig. 3E, Table 2A). Neurocan-positive fluorescence intensity in L1 was very high compared with that in the other layers (Fig. 3F, Table 2A). Brevican-positive fluorescence intensity in L4 was high compared with that in L1, L5 A, L5B, and L6 (Fig. 3G, Table 2A). Cat-315-positive fluorescence intensity in L4 was very high compared with that in the other layers (Fig. 3H, Table 2A).

In the mouse piriform cortex, the fluorescence intensity of ECM molecules also showed significant variation among the layers at 11 w. WFA-positive fluorescence intensity in L1A was significantly high compared with that in the other layers (Fig. 4A, Table 2B). HABP-positive fluorescence intensity in L3 was very high compared with that in the other layers (Fig. 4B, Table 2B). Hapln1-positive fluorescence intensity in L1A was very high compared with that in the other layers (Fig. 4C, Table 2B). Tenascin-R-positive fluorescence intensity in L1A and L3 was high compared with that in L1B and L2 (Fig. 4D, Table 2B). Both AB1031- and Neurocan-positive fluorescence intensities in L1A were very high compared with that in the other layers (Fig. 4E, F Table 2B). Neurocan-positive fluorescence intensity in L2 was low compared with that in the other layers. Brevican-positive fluorescence intensity in L1A was very high compared with that in the other layers (Fig. 4G, Table 2B). Cat-315-positive fluorescence intensity in L1A was very high compared with that in the other layers (Fig. 4H, Table 2B).

ECM molecules in L1A of the mouse piriform cortex

As many ECM molecules were expressed in L1A of the mouse piriform cortex at high concentration, we observed ECM molecules at high magnification. High magnification images revealed WFA, HABP, Hapln1, tenascin-R, AB1031, neurocan, brevican, and Cat-315-positive molecules scattered throughout L1A (Fig. 5A–G, A'-G'). WFA-positive molecules did not colocalize with HABP, Hapln1, tenascin-R, AB1031, neurocan, brevican, and Cat-315-positive molecules in L1A of the mouse piriform cortex at 11 w (Fig. 5A"–G").

GABAergic and glutamatergic synaptic terminals in the mouse somatosensory and piriform cortices

To investigate the distribution relationship between the synaptic terminal and ECM molecules, we labeled both GAD67-positive synaptic terminals and VGLUT1-positive synaptic terminals (Fig. 6A–D). GAD67- and VGLUT1-positive synaptic terminals were expressed in the neuropil

Table 2
p values for Figs. 3, 4, and 6.

fluorescence intensity (a.u.)										
			WFA	HABP	Hapln1	Tenascin-R	AB1031	Neurocan	Brevican	Cat-315
A: Fig. 3										
L1	vs	L2/3	< 0.001	0.003	< 0.001	0.848	< 0.001	< 0.001	< 0.001	0.007
L1	vs	L4	< 0.001	0.904	< 0.001	0.123	< 0.001	< 0.001	< 0.001	< 0.001
L1	vs	L5 A	< 0.001	0.006	0.003	0.165	< 0.001	< 0.001	0.055	0.594
L1	vs	L5B	< 0.001	0.083	< 0.001	0.053	< 0.001	< 0.001	< 0.001	< 0.001
L1	vs	L6	< 0.001	0.095	0.816	0.881	0.011	< 0.001	0.905	0.142
L2/3	vs	L4	< 0.001	0.005	< 0.001	0.083	< 0.001	0.17	0.053	< 0.001
L2/3	vs	L5 A	< 0.001	0.839	0.038	0.231	0.562	< 0.001	0.002	0.029
L2/3	vs	L5B	< 0.001	< 0.001	0.867	0.034	0.001	0.173	0.654	0.163
L2/3	vs	L6	< 0.001	0.191	< 0.001	0.733	0.042	0.082	< 0.001	< 0.001
L4	vs	L5 A	< 0.001	0.009	< 0.001	0.004	< 0.001	0.032	< 0.001	< 0.001
L4	vs	L5B	< 0.001	0.064	< 0.001	0.691	0.002	0.007	0.018	< 0.001
L4	vs	L6	< 0.001	0.121	< 0.001	0.164	< 0.001	0.711	< 0.001	< 0.001
L5 A	vs	L5B	0.896	< 0.001	0.025	0.001	< 0.001	< 0.001	0.007	< 0.001
L5 A	vs	L6	< 0.001	0.269	0.001	0.124	0.145	0.075	0.071	0.046
L5B	vs	L6	< 0.001	0.001	< 0.001	0.074	< 0.001	0.002	< 0.001	< 0.001
B: Fig. 4										
L1A	vs	L1B	< 0.001	< 0.001	< 0.001	< 0.001	< 0.001	< 0.001	< 0.001	< 0.001
L1A	vs	L2	< 0.001	< 0.001	< 0.001	< 0.001	< 0.001	< 0.001	< 0.001	< 0.001
L1A	vs	L3	< 0.001	< 0.001	< 0.001	0.118	< 0.001	< 0.001	< 0.001	< 0.001
L1B	vs	L2	0.008	0.019	< 0.001	< 0.001	< 0.001	< 0.001	0.004	0.042
L1B	vs	L3	0.007	< 0.001	< 0.001	< 0.001	< 0.001	0.95	0.052	0.08
L2	vs	L3	0.928	< 0.001	0.048	< 0.001	0.001	< 0.001	0.359	< 0.001

fluorescence intensity (a.u.)				
			GAD67	VGLUT1
C: Fig. 6 (E, F)				
L1	vs	L2/3	< 0.001	< 0.001
L1	vs	L4	< 0.001	< 0.001
L1	vs	L5 A	< 0.001	< 0.001
L1	vs	L5B	< 0.001	< 0.001
L1	vs	L6	< 0.001	< 0.001
L2/3	vs	L4	< 0.001	< 0.001
L2/3	vs	L5 A	< 0.001	0.697
L2/3	vs	L5B	0.364	< 0.001
L2/3	vs	L6	< 0.001	0.04
L4	vs	L5 A	< 0.001	0.02
L4	vs	L5B	< 0.001	1
L4	vs	L6	< 0.001	0.549
L5 A	vs	L5B	< 0.001	0.016
L5 A	vs	L6	< 0.001	0.648
L5B	vs	L6	< 0.001	0.491
D: Fig. 6 (G, H)				
L1A	vs	L1B	< 0.001	0.669
L1A	vs	L2	< 0.001	< 0.001
L1A	vs	L3	< 0.001	0.052
L1B	vs	L2	< 0.001	< 0.001
L1B	vs	L3	0.224	0.465
L2	vs	L3	< 0.001	< 0.001

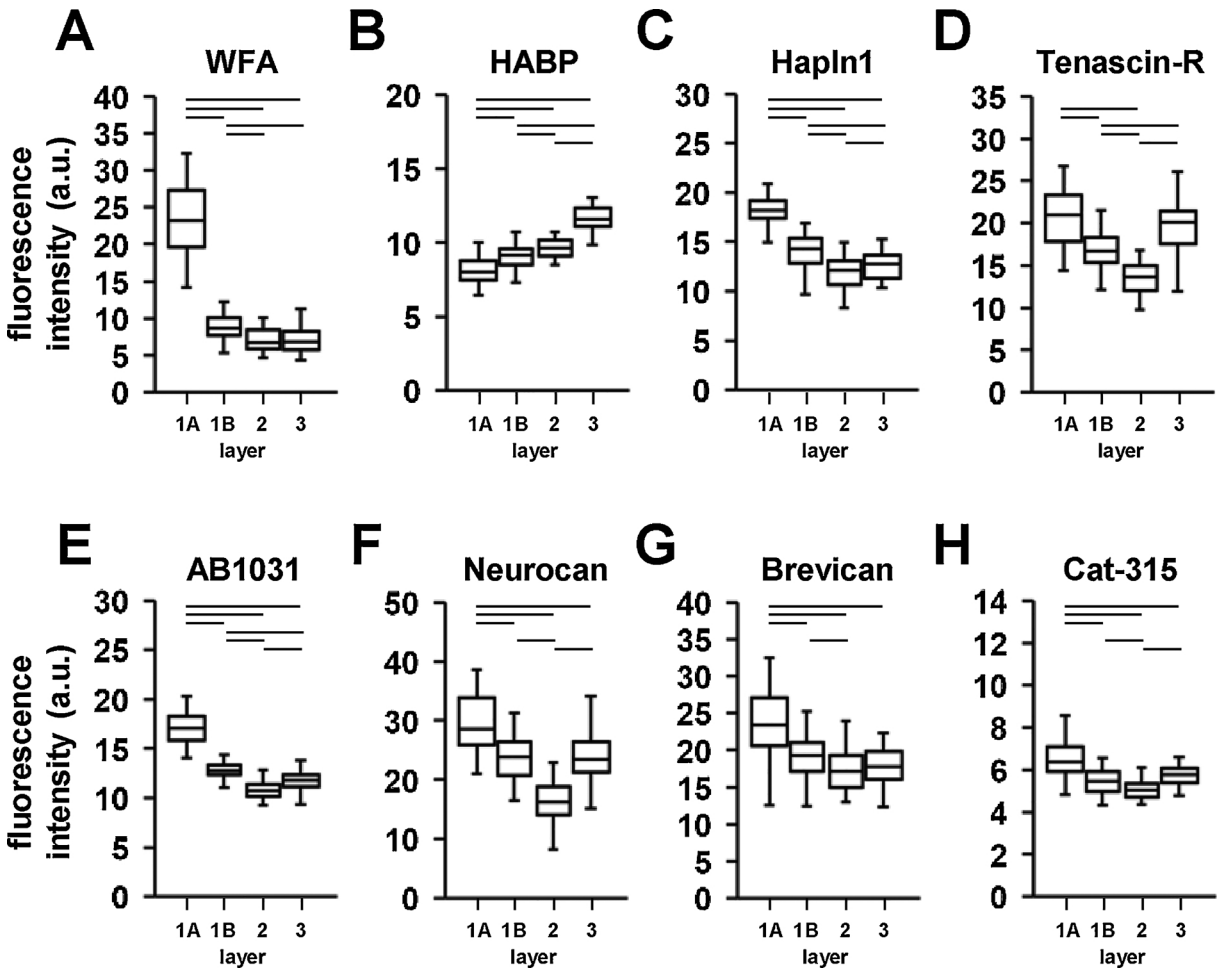

Fig. 4. Quantitative analyses of extracellular matrix molecules in the mouse piriform cortex.
Quantified mean fluorescence intensity of WFA-positive molecules (A), HABP-positive molecules (B), Hapln1-positive molecules (C), tenascin-R-positive molecules (D), AB1031-positive molecules (E), neurocan-positive molecules (F), brevican-positive molecules (G), and Cat-315-positive molecules (H), excluding the PNN, in the mouse piriform cortex at postnatal week 11. Data are expressed as box plots. *$p < 0.05$ for comparison between layers. The respective p values are listed in Table 2. WFA: $F_{(3,179)} = 354.682$, $p < 0.001$ in.(A). HABP: $F_{(3,95)} = 68.170$, $p < 0.001$ in.(B). Hapln1: $F_{(3,191)} = 126.329$, $p < 0.001$ in.(C). tenascin-R: $F_{(3,143)} = 42.447$, $p < 0.001$ in.(D). AB1031: $F_{(3,155)} = 221.711$, $p < 0.001$ in.(E). neurocan: $F_{(3,143)} = 54.192$, $p < 0.001$ in.(F). brevican: $F_{(3,167)} = 28.465$, $p < 0.001$ in.(G). Cat-315: $F_{(3,143)} = 30.712$, $p < 0.001$ in.(H).

of the mouse somatosensory and piriform cortices at 11 w (Fig. 6A–D). Their distribution pattern was also region-specific and layer-specific (Fig. 6A–D). We quantified layer-specific GAD67- and VGLUT1-positive signal intensities, excluding GAD67-positive neurons, in the somatosensory cortex (Fig. 6E, F, Table 2C) and piriform cortex (Fig. 6G, H, Table 2D). In the somatosensory cortex, GAD67-positive fluorescence intensity in L4 was very high compared with that in the other layers (Fig. 6E, Table 2C). GAD67-positive fluorescence intensity in L1 was low compared with that in the other layers. VGLUT1-positive fluorescence intensity in L1 was very high compared with that in the other layers (Fig. 6F, Table 2C). In the piriform cortex, GAD67-positive fluorescence intensity in L1A was very high compared with that in the other layers (Fig. 6G, Table 2D). VGLUT1-positive fluorescence intensity in L2 was very low compared with that in the other layers (Fig. 6H, Table 2D).

High magnification showed that GAD67- and VGLUT1-positive synaptic terminals were scattered throughout the cortical layers in granular form in the mouse somatosensory cortex (Fig. 7A–L). These GAD67- and VGLUT1-positive synaptic terminals did not colocalize with WFA-positive molecules in all layers of the mouse somatosensory cortex (Fig. 7A''–L''). In addition, GAD67- and VGLUT1-positive synaptic terminals were also present in PNNs (Fig. 7M–N, M'–N', M''–N'').

As GAD67- and VGLUT1-positive molecules were expressed in L1A of the mouse piriform cortex at high concentration, we observed these synaptic terminals at high magnification (Fig. 5H, I). GAD67- and VGLUT1-positive synaptic terminals did not colocalize with WFA-positive molecules in L1A of the mouse piriform cortex (Fig. 5H'', I'').

Effect of aging on WFA-positive molecules in the mouse somatosensory and piriform cortices

Next, we examined the developmental expression of WFA-positive molecules in the somatosensory and piriform cortices with age. WFA-positive molecules were already present in both cortices at 2 w (Fig. 8A–C). We observed that WFA-positive intensity at 2 w was weak within the somatosensory and piriform cortices compared to the intensity in both cortices at 11 w (Fig. 8A–C). Intense WFA-positive signal intensity was seen in L1A of the piriform cortex at 4 w (Fig. 8C). WFA-positive signal intensity in both cortices significantly decreased from 11 w to 2y (Fig. 8A–C).

We observed the formation of reticular-like WFA-positive PNNs in these cortices with age (Fig. 8D, E). At 2 w, in the somatosensory cortex, WFA-positive PNNs showed attenuated staining. WFA-positive PNNs were sparse and less condensed in L2/3 of the somatosensory cortex at 2 w (Fig. 8D). At 11 w, WFA-positive PNNs exhibited a clear condensed reticular-like structure (Fig. 8D). At 2 w, WFA-positive PNNs were not

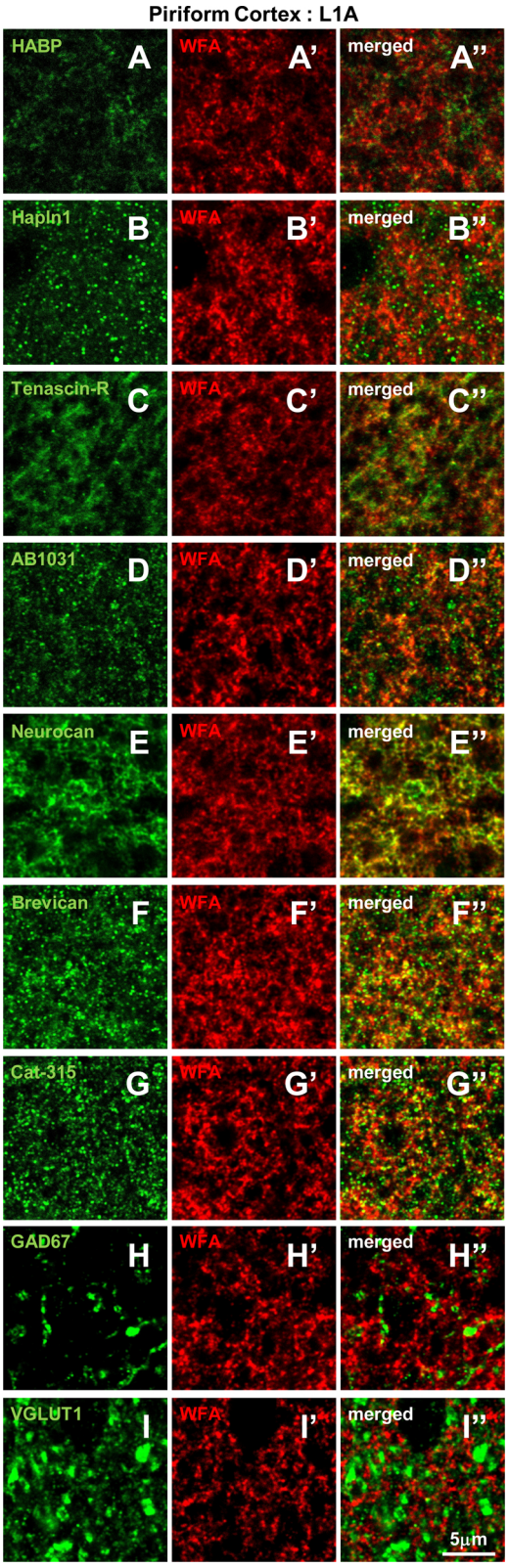

Fig. 5. Colocalization of extracellular matrix molecules and WFA in the mouse piriform cortex.
Double confocal images of HABP (A), Hapln1 (B), tenascin-R (C), AB1031 (D), neurocan (E), brevican (F), Cat-315 (G), GAD67 (H), VGLUT1 (I), WFA (A'–I'), and merged images (A''–I'') in the upper level of L1 of the mouse piriform cortex at postnatal week 11. Scale bars: 5 μm in I'' (applies to A–I, A'–I', A''–I'').

observed in the piriform cortex (Fig. 8C), but were present at 4 w (Fig. 8C, E). We observed WFA-positive molecules in L1A of the piriform cortex at 2 w (Fig.8C, E). Intense WFA-positive signal intensity was seen in L1A of the piriform cortex at 4 w (Fig. 8E). At 11 w, WFA-positive PNNs in L3 of the piriform cortex showed condensed staining compared to that at 4 w. WFA-positive signal intensity in L3 of the piriform cortex significantly decreased from 11 w to 2y.

Quantitative analysis of WFA-positive PNNs and WFA-positive molecules in the mouse somatosensory cortex with age

First, we quantified WFA-positive PNNs in the mouse somatosensory cortex (Fig. 9A, Table 3A). The mean WFA-positive PNN density increased between 2 w and 2y. The density of WFA-positive PNNs significantly increased in L4 of the somatosensory cortex.

To analyze the effect of aging on the expression of WFA-positive molecules, we analyzed the fluorescence intensity of each WFA-positive PNN in the mouse somatosensory cortex with age (Fig. 9B, Table 3B). The mean fluorescence intensity of WFA-positive PNNs increased between 2 w and 2y. The fluorescence intensity of WFA-positive PNNs differed in each of the cortical layers and at each age.

Next, we analyzed WFA-positive molecules, excluding PNNs, in the mouse somatosensory cortex with age (Fig. 9C, Table 3C). The mean fluorescence intensity of WFA-positive molecules, excluding PNNs, increased between 2 w and 3 w. In L1, 2/3, and 5 A, we observed a significant decrease in the fluorescence intensity of WFA-positive molecules, excluding PNNs, between 11 w and 2y. In L4, 5B, and L6, there was an increase in the fluorescence intensity of WFA-positive molecules, excluding PNNs, between 1y and 2y.

Quantitative analysis of WFA-positive PNNs and WFA-positive molecules in the mouse piriform cortex with age

We quantified WFA-positive PNNs in the mouse piriform cortex (Fig. 10A, Table 3D). The mean WFA-positive PNNs density increased between 3 w and 11 w. The density of WFA-positive PNNs significantly decreased in the piriform cortex.

Next, we analyzed the fluorescence intensity of each WFA-positive PNN in the mouse piriform cortex with age (Fig. 10B, Table 3E). The mean fluorescence intensity of WFA-positive PNNs increased between 3 w and 11 w. There was a decrease in the fluorescence intensity of WFA-positive PNNs between 11 w and 2y.

We analyzed WFA-positive molecules excluding PNNs in the mouse piriform cortex with age (Fig. 10C, Table 3F). In L1A, the mean fluorescence intensity of WFA-positive molecules, excluding PNNs, increased between 2 w and 4 w. In L1B, L2, and L3, the mean fluorescence intensity of WFA-positive molecules, excluding PNNs, increased between 2 w and 11 w. In all layers, we observed a significant decrease in the fluorescence intensity of WFA-positive molecules, excluding PNNs, between 11 w and 2y.

Discussion

In this study, we analyzed the expression levels of WFA-positive molecules, aggrecan, brevican, neurocan, tenascin-R, Hapln1, and hyaluronic acid, in each layer of the somatosensory and piriform cortices of mature mice using histochemical and immunohistological techniques. In the mature mouse cortex, these ECM molecules showed brain region-specific, layer-specific, and ECM molecule-specific expression. High magnification observation by confocal laser microscopy revealed that ECM molecules are present in the extracellular region at high density in the mature cortex, in addition to the PNN area. In addition, the WFA-positive molecules existing outside the PNN area showed region-dependent variation with age.

The expression level of ECM molecules was lower in the other regions than in the PNN area, but there were no layers without ECM

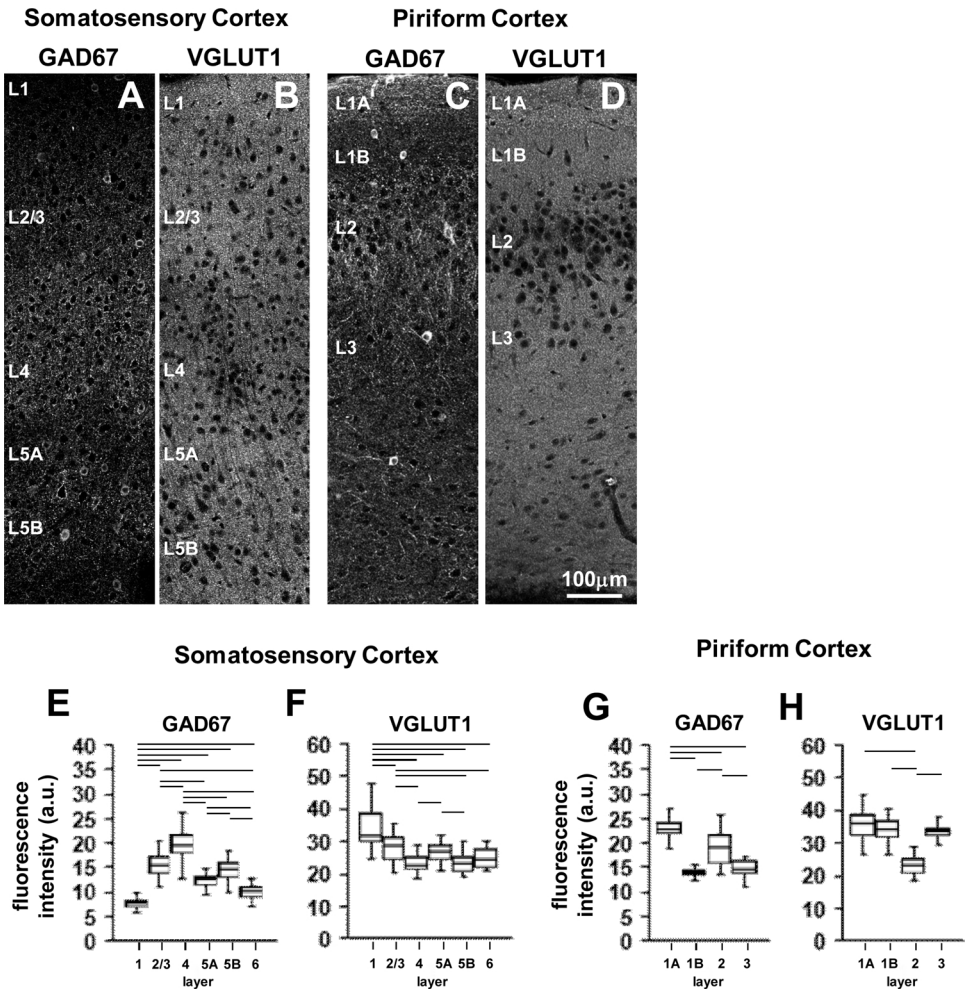

Fig. 6. GAD67-positive and VGLUT1-positive puncta in the mouse somatosensory and piriform cortices.
Representative images show the laminar distribution of GAD67-positive puncta (A) and VGLUT1-positive puncta (B) in the mouse somatosensory cortex at postnatal week 11. Representative images show the laminar distribution of GAD67-positive puncta (C) and VGLUT1-positive puncta (D) in the mouse piriform cortex at postnatal week 11. Scale bars: 100 μm in D (applies to A–D). Quantified mean fluorescence intensity of GAD67-positive puncta (E) and VGLUT1-positive puncta (F), excluding the GAD67-positive neurons, in the mouse somatosensory cortex at postnatal week 11. Quantified mean fluorescence intensity of GAD67-positive puncta (G) and VGLUT1-positive puncta (H), excluding the GAD67-positive neurons, in the mouse piriform cortex at week 11. Data are expressed as box plots. *$p < 0.05$ for comparison between layers. The respective p values are listed in Table 2.
GAD67: $F_{(5,239)} = 148.527$, $p < 0.001$ in.(E).
VGLUT1: $F_{(5,143)} = 28.293$, $p < 0.001$ in.(F).
GAD67: $F_{(3,127)} = 63.110$, $p < 0.001$ in.(G).
VGLUT1: $F_{(3,111)} = 60.856$, $p < 0.001$ in.(H).

molecules. In the extracellular region outside the PNN area, it is presumed that migration is difficult for neurons and glial cells with a diameter of approximately 10 μm. Even axons with a diameter of 1–2 μm are unlikely to easily outgrow. It has been widely reported that neuronal plasticity is restored by ChABC injection in the CNS (Pizzorusso et al., 2006; Gogolla et al., 2009; de Vivo et al., 2013; Senkov et al., 2014). These reports have indicated that PNN destruction by ChABC is the mechanism underlying neural plastic resurgence. ChABC removes the CS chain from the lectican core protein. However, the present study revealed that there are numerous WFA-positive molecules (CS chains) other than in the PNN area. That is, at the time of ChABC treatment, it is suggested that not only PNNs, but also other WFA-positive molecules are subjected to enzyme treatment. It is obvious that axon elongation is also facilitated if ECM molecules in the extracellular region are removed by ChABC. Moreover, in mice lacking specific PNN components, such as Crtl1, PNN formation decreases and neural plasticity increases (Carulli et al., 2010). PNN formation is reduced in cultured neurons of neurocan-, brevican-, or TN-R-deficient mice. In these neurons, changed synaptic plasticity, decreased synaptogenesis, decreased synaptic stability, and decreased synaptic activity are observed (Geissler et al., 2013). In these reports, changes, such as in synaptic plasticity, attributable to lack of ECM molecules are only suggested due to impaired PNN formation. However, considering the results of this study, ECM molecules, other than the PNN area, also lack expression in these deficient mice. Therefore, it is possible that ECM malfunction involved in other areas may be implicated in the increase in neural plasticity. This study suggests that further research to reconsider the mechanism of reactive neuronal plasticity is necessary.

Each component of the ECM molecule showed layer-dependent distribution. These characteristic layer-specific expressions indicate that ECM molecules play diverse roles in these layers. ECM structure in the brain has also been shown to function as a physical barrier to prevent lateral diffusion of AMPA receptors in postsynaptic sites (Frischknecht et al., 2009; Frischknecht and Gundelfinger, 2012). In addition, ECM molecules have been reported to regulate several ion channels; for example, tenascin-R regulates sodium channels (Srinivasan et al., 1998). Furthermore, hyaluronic acid regulates L-type calcium and potassium channels (Davis et al., 2002; Evers et al., 2002; Kochlamazashvili et al., 2010). Brevican has been shown to be significantly involved in nerve excitability in the axon initial segment (John et al., 2006). CSPG regulates the diffusion of Ca^{2+} in brain tissue (Hrabetová et al., 2009). We also showed that both the GAD67-positive inhibitory synaptic terminal and the VGLUT1-positive excitatory synaptic terminal were differentially expressed in each brain area and each layer. This result shows that the neuronal transmitters and receptors are region-specific and layer-specific. That is, if neurotransmitters and excitability differ in each brain region and layer, ECM molecules playing roles in that region and layer would also differ. The results of this study are consistent with those of previous reports. Further studies are needed to analyze the function of each ECM molecule in the synaptic cleft.

On the other hand, we did not control for the differences in cell density, soma shape/size and layer volumes. The difference in cell density, cell shape/size, and layer volume may have influenced the present results. We used same analytical method as other studies demonstrating the distribution of molecules in the extracellular region of the CNS (Barker et al., 2012; Risher et al., 2014; Moyer et al., 2016; Sceniak et al., 2016; Bolós et al., 2018). In order to clarify the difference

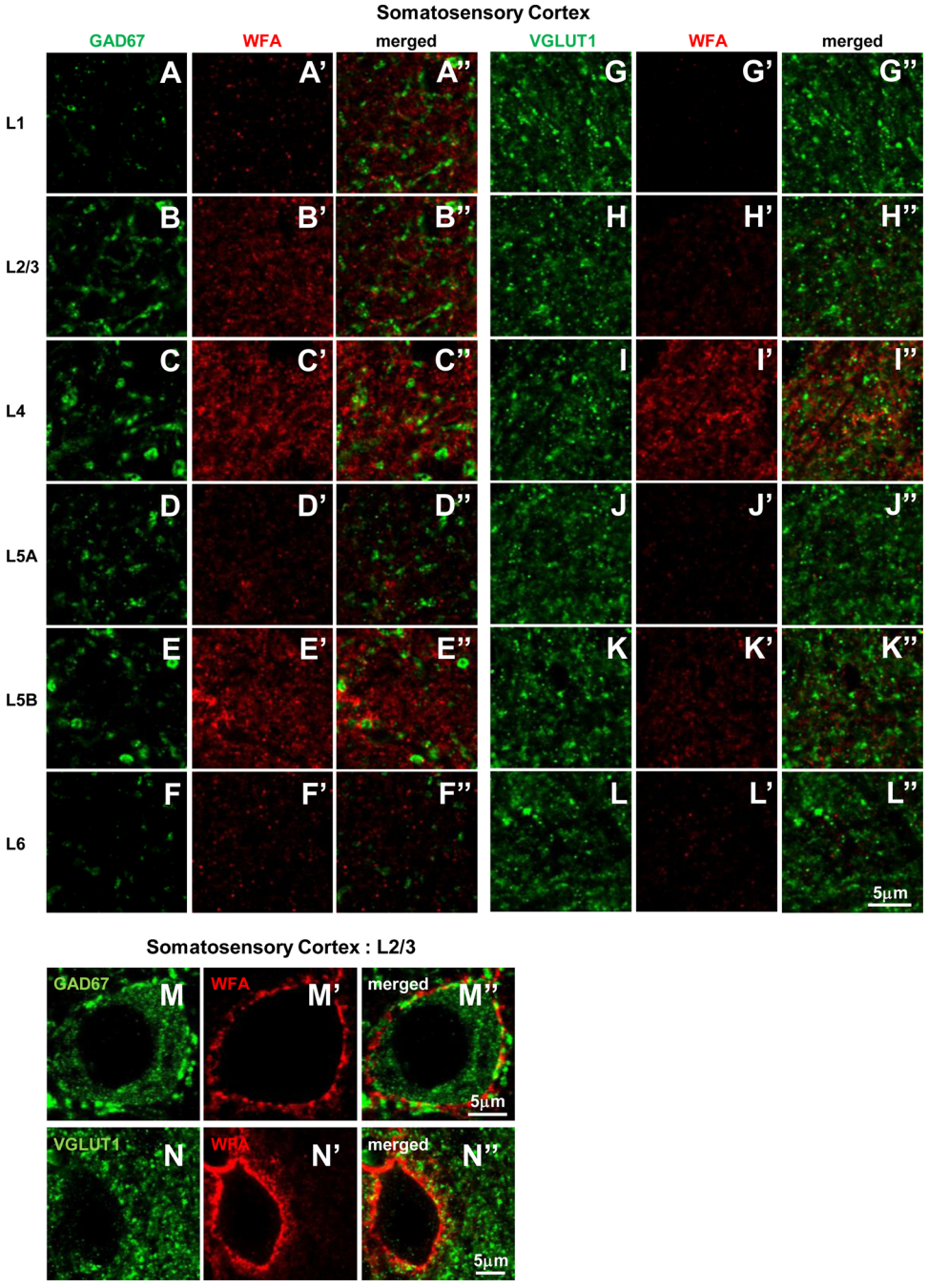

Fig. 7. Distribution of GAD67-positive and VGLUT1-positive puncta in the mouse somatosensory cortex.
Double confocal images of GAD67 (A–F), WFA (A'–F') , and merged images (A''–F'') in L1 (A, A', A''), L2/3 (B, B', B''), L4 (C, C', C''), L5 A (D, D', D''), L5B (E, E', E''), and L6 (F, F', F'') of the mouse somatosensory cortex at postnatal week 11. Double confocal images of VGLUT1 (G–L), WFA (G'–L'), and merged images (G''–L'') in L1 (G, G', G''), L2/3 (H, H', H''), L4 (I, I', I''), L5 A (J, J', J''), L5B (K, K', K''), and L6 (L, L', L'') of the mouse somatosensory cortex at postnatal week 11. The same capture conditions were used for all section images. High-magnification double confocal images of GAD67 (M), WFA (M'), and merged image (M'') around PNNs in L2/3 of the mouse somatosensory cortex at postnatal week 11. High-magnification double confocal images of VGLUT1 (N), WFA (N'), and merged image (N'') around PNNs in L2/3 of the mouse somatosensory cortex at postnatal week 11. Scale bars: 5 μm in L'' (applies to A–L, A'–L', A''–L''); 5 μm in M'' (applies to M, M', M''); 5 μm in N'' (applies to N, N', N'').

in layer-specific expressions of ECM molecules in each layer, it is necessary to consider cell density, soma shape/size and layer volumes.

L4 in the somatosensory cortex receives direct inputs from the thalamus and then conveys that information to L2/3 (Winer et al., 2005; Schiff and Reyes, 2012). In L4 of the somatosensory cortex, the GAD67-positive synaptic terminal is expressed at high density and the excitation by the input from the hypothalamus is inhibited (Jiao et al., 2006). In this study, it is speculated that WFA-positive molecules, aggrecan, Hapln1, and brevican, are highly expressed in L4 compared to the other layers and that they play a role in synaptic transmission. Additionally, L4 is a region with many PV-positive neurons surrounded by PNNs (McRae et al., 2007). High ECM expression in L4 may be due to high PNN density. However, why PNNs with ECM molecules accumulate around PV-positive neurons remains unknown, but it is reportedly related to the electrical characteristics of fast-spiking neurons (Morris and Henderson, 2000).

The piriform cortex is associated with the sensory cortex, which is indispensable for recognition and odor memory (Isaacson, 2010; Bekkers and Suzuki, 2013). Interestingly, the piriform cortex shows long-term plasticity (Strauch and Manahan-Vaughan, 2018). However, it is also a brain region where abnormalities are seen in patients with epilepsy and AD (Li et al., 2010; Vaughan and Jackson, 2014). We found high expression of ECM molecules in L1 of the piriform cortex compared with that in the other layers. L1 of the cortex is a special layer with no pyramidal cells present. L1 has axons from 2 to 6 layers of pyramidal cells and of inhibitory interneurons from other cortical regions (Felleman et al., 1991; Vogt et al., 1991). Glutamatergic, GABAergic, cholinergic, noradrenergic, and serotoninergic axons coexist in L1 on the apical dendrites of pyramidal cells of 2–6 layers (Vogt et al., 1991). Consistent with these reports, our results showed that both GAD67- and VGLUT1-positive synaptic terminals were more highly expressed in this than in the other layers. It is suggested that the ECM

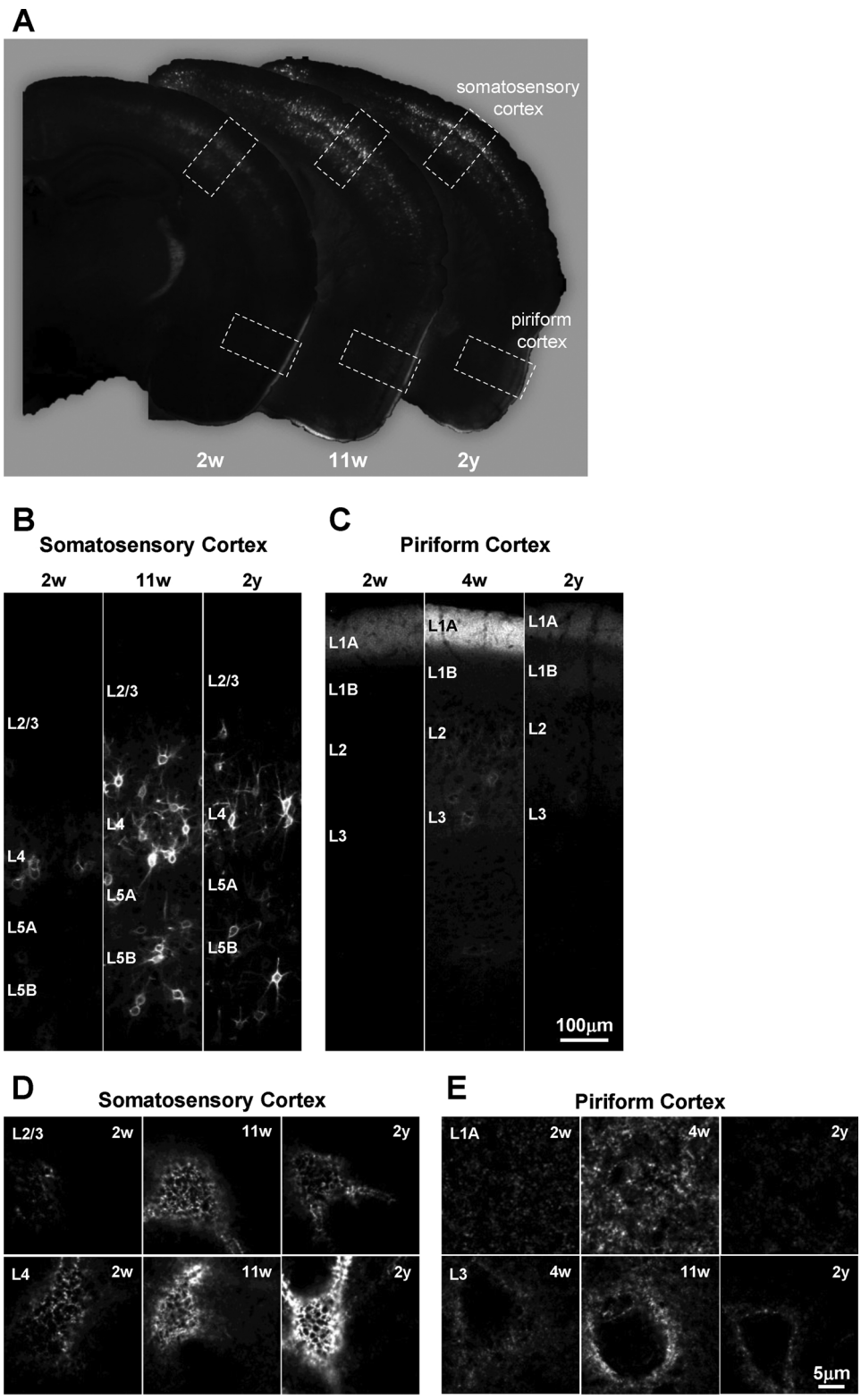

Fig. 8. The effect of aging on WFA-positive molecules in the mouse somatosensory and piriform cortices.
Representative whole-brain sections labeled for WFA in 2-week-old (A, left panels), 11-week-old (A, central panels), and 2-year-old mice (A, right panels). Representative images show the laminar distribution of WFA-positive molecules in the mouse somatosensory cortex (B) and piriform cortex (C). The same capture conditions were used for all section images. Representative morphologies of WFA-positive PNNs in L2/3 (D, upper layers) and L4 (D, down layers) of the somatosensory cortex. Representative distribution of WFA-positive molecules in L1A (E, upper layers) and WFA-positive PNN L3 (E, down layers) of the piriform cortex. Scale bars: 100 μm in C (applies to B–C); 5 μm in E (applies to D–E).

molecules showed high expression level due to the high density of synaptic terminals in L1A. ECM molecules formed in the synaptic cleft restrict spine dynamics and functional plasticity (Levy et al., 2014). Therefore, if abnormality occurs in ECM molecules in L1A of the piriform cortex, spine and synaptic transmission abnormalities will also occur. Studies to analyze the association between L1 synapse of the piriform cortex and the ECM molecule are necessary.

In the somatosensory cortex, the number of WFA-positive PNNs, WFA-positive PNN fluorescence intensity, and WFA-positive ECM molecule fluorescence intensity increased with age. It is generally known that neuronal plasticity decreases with aging (Burke and Barnes, 2006). Compared with young adult mice, in aged mice, the number of WFA-positive PNNs increases in the somatosensory cortex (Karetko-Sysa et al., 2014; Ueno et al., 2018). WFA-positive PNNs are formed at the final stage of maturation of the inhibitory neuronal circuit, and WFA-positive PNN expression is confirmed approximately 2 weeks after birth

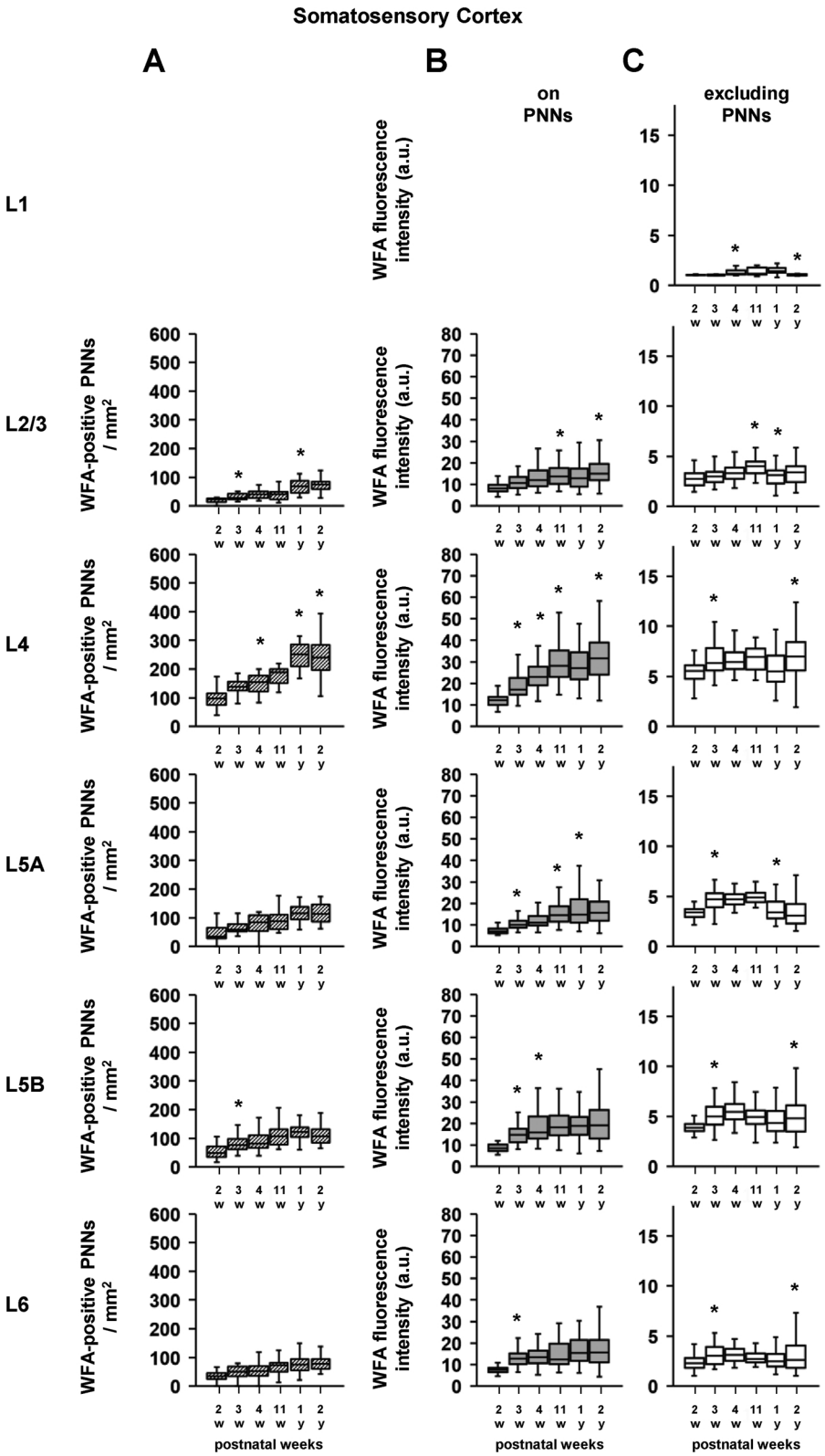

Fig. 9. Quantitative analyses of layer-specific aging patterns of WFA-positive molecules and WFA-positive PNNs in the mouse somatosensory cortex.
Quantified density of WFA-positive PNNs (A), mean fluorescence intensity of WFA-positive PNNs (B), and mean fluorescence intensity of WFA-positive molecules, excluding the PNN, (C) in L1, L2/3, L4, L5 A, L5B, and L6 of the mouse somatosensory cortex. Data are expressed as box plots. Statistical significance is represented by asterisks: *p < 0.05. Statistically significant differences were compared with earlier age groups. The respective p values are listed in Table 3. L2/3: $F_{(5,113)}$ = 22.506, p < 0.001, L4: $F_{(5,113)}$ = 28.311, p < 0.001, L5 A: $F_{(5,113)}$ = 11.581, p < 0.001, L5B: $F_{(5,113)}$ = 7.609, p < 0.001, L6: $F_{(5,113)}$ = 6.063, p < 0.001 in.(A). L2/3: $F_{(5,411)}$ = 12.232, p < 0.001, L4: $F_{(5,692)}$ = 101,085, p < 0.001, L5 A: $F_{(5,457)}$ = 31.012, p < 0.001, L5B: $F_{(5,527)}$ = 26.022, p < 0.001, L6: $F_{(5,455)}$ = 16.322, p < 0.001 in.(B). L1: $F_{(5,344)}$ = 21.885, p < 0.001, L2/3: $F_{(5,344)}$ = 8.021, p < 0.001, L4: $F_{(5,344)}$ = 7.905, p < 0.001, L5 A: $F_{(5,344)}$ = 26.901, p < 0.001, L5B: $F_{(5,344)}$ = 8.153, p < 0.001, L6: $F_{(5,344)}$ = 4.535, p = 0.001 in.(C).

in the mouse somatosensory cortex (Ueno et al., 2017). Increase in the number of WFA-positive PNNs, WFA-positive PNN fluorescence intensity, and WFA-positive ECM molecule fluorescence intensity indicates decrease in plasticity of the somatosensory cortex.

Conversely, in the piriform cortex, unlike the somatosensory cortex, WFA-positive PNN number, WFA-positive PNN fluorescence intensity, and WFA-positive ECM molecule fluorescence intensity increased 11 weeks after birth but decreased thereafter. These changes were not reflected in the somatosensory cortex. Considering that the ECM molecule has plastic and neuroprotective functions, it is speculated that plasticity and vulnerability increase in the piriform cortex of aged mice. Studies have reported that the piriform cortex shows long-term plasticity (Strauch and Manahan-Vaughan, 2018) and that the piriform cortex becomes a pathogenic region of AD due to aging (Li et al., 2010;

Table 3
p values for Figs. 9 and 10.

A: Fig. 9A

WFA-positive PNNs / mm^2

			L1	L2/3	L4	L5 A	L5B	L6
2 w	vs	3 w		0.052	0.021	0.135	0.025	0.172
3 w	vs	4 w		0.273	0.495	0.383	0.504	0.999
4 w	vs			0.731	0.004	0.096	0.314	0.248
11 w	vs	1y		< 0.001	0.014	0.257	0.182	0.274
1y	vs	2y		0.569	0.841	0.519	0.442	0.55

B: Fig. 9**B**

WFA fluorescence intensity on PNNs (a.u.)

			L1	L2/3	L4	L5 A	L5B	L6
2 w	vs	3 w		0.059	< 0.001	0.005	< 0.001	< 0.001
3 w	vs	4 w		0.064	< 0.001	0.102	0.006	0.258
4 w	vs	11 w		0.012	< 0.001	< 0.001	0.22	0.793
11 w	vs	1y		0.072	0.174	0.028	0.73	0.222
1y	vs	2y		0.013	< 0.001	0.971	0.166	0.284

C: Fig. 9**C**

WFA fluorescence intensity excluding PNNs (a.u.)

			L1	L2/3	L4	L5A	L5B	**L6**
2 w	vs	3 w	0.77	0.116	0.001	< 0.001	< 0.001	< 0.001
3 w	vs	4 w	< 0.001	0.24	0.733	0.572	0.263	0.676
4 w	vs	11 w	0.536	0.001	0.645	0.206	0.118	0.165
11 w	vs	1y	0.024	< 0.001	0.005	< 0.001	0.095	0.693
1y	vs	2y	< 0.001	0.056	< 0.001	0.509	0.01	0.041

D: Fig. 10**A**

WFA-positive PNNs / mm^2

			L1A	L1B	L2	L3
3 w	vs	4 w			0.966	0.032
4 w	vs	11 w			0.039	< 0.001
11 w	vs	1y			0.969	0.095
1y	vs	2y			< 0.001	< 0.001

E: Fig. 10**B**

WFA fluorescence intensity on PNNs (a.u.)

			L1A	L1B	L2	L3
3 w	vs	4 w			< 0.001	
4 w	vs	11 w			< 0.001	< 0.001

(*continued on next page*)

Table 3 (*continued*)

E: Fig. 10**B**

WFA fluorescence intensity on PNNs (a.u.)

			L1A	L1B	L2	L3
11 w	vs	1y			0.085	< 0.001
1y	vs	2y			< 0.001	< 0.001

F: Fig. 10**C**

WFA fluorescence intensity excluding PNNs (a.u.)

			L1A	L1B	L2	**L3**
2 w	vs	3 w	< 0.001	0.088	0.005	0.063
3 w	vs	4 w	< 0.001	< 0.001	< 0.001	< 0.001
4 w	vs	11 w	< 0.001	< 0.001	< 0.001	< 0.001
11 w	vs		< 0.001	0.198	0.004	< 0.001
1y	vs	2y	< 0.001	0.021	< 0.001	< 0.001

Vaughan and Jackson, 2014). The present results will be useful for elucidating these mechanisms, and further research is needed to determine the cause of neurodegenerative disease in the piriform cortex.

It has been reported that ECM molecules inhibit axonal outgrowth after brain trauma (McKeon et al., 1991; Silver, 1994; Asher et al., 2001; McKeon et al., 1995). Changes in ECM molecules in the brain have also been reported in AD (Bonneh-Barkay and Wiley, 2009), schizophrenia (Berretta, 2012), autism (Mercier et al., 2012), and epilepsy (Dityatev, 2010; Pitkänen et al., 2014). It is clear that ECM molecules are somehow related to these diseases. Studies on brain trauma employing $FeCl_3$ injections have shown that the size of brain injury increases in aggrecan-, Hapln1-, and tenascin-R-deficient mice compared to wild-type mice, and it has been suggested that these ECM molecules are associated with diffusion properties (Suttkus et al., 2014). Interestingly, it has also been reported that neuronal sensitivity to brain injury differs depending on the brain region. Although the mechanism of this phenomenon has not been elucidated, there is a possibility that it involves differences in the distribution of ECM molecules. It is also known that neurons covered with PNN are less susceptible to accumulation of tau protein (Suttkus et al., 2016a,b). Reportedly, aggregation of tau protein leads to further aggregation of tau protein, and extracellular tau protein species spread to neighboring cells in neurodegenerative disease (Clavaguera et al., 2009; Frost et al., 2009; Kfoury et al., 2012), which shows that ECM molecules are related to aggregation of tau protein. In postmortem brain studies of patients with schizophrenia, WFA-positive PNNs were found to decrease only in the frontal cortex, entorhinal cortex, and amygdala (Pantazopoulos et al., 2010; Mauney et al., 2013). The findings of these clinical studies indicate region-specific abnormalities of CSPG. It is highly possible that the brain region-specific ECM components and ECM expression levels shown in the present study are involved in these neurodegenerative and neuropsychiatric diseases and in brain trauma. Especially, the human cortex has a higher proportion of extracellular region compared to the mouse cortex. Therefore, it is presumed that the change in ECM in the extracellular region has a greater impact on neurons in humans than in mice. Further research to clarify the relationship between the ECM and these diseases is necessary.

We demonstrated brain region-specific and layer-specific expression of ECM molecules in the mature mouse cortex for the first time. It is suggested that these characteristic expressions of ECM molecules reflect specific functions of neurons, glia, and synaptic terminals present in each region. In addition, the specific distribution of ECM molecules with plasticity regulation and neuroprotective functions suggests that plasticity and vulnerability differ in each brain region and each layer. In addition, changes in ECM molecules due to aging significantly differed in each brain region. Knowledge of the detailed expression of ECM molecules under normal conditions would facilitate detection of cortical changes associated with neuropsychiatric disorders and neurodegenerative diseases.

Author contributions

All authors had full access to all the study data and take full responsibility for the integrity of the data and the accuracy of the data analysis. Study concept and design: H.U. and M.O. Data acquisition: H.U. and S.S. Data analysis and interpretation: H.U. and S.S. Drafting of the manuscript: H.U. and M.O. Critical revision of the manuscript for important intellectual content: S.M., N.K., K.W., Y.M., and T.I. Statistical analyses: H.U and S.S. Study supervision: M.O. and T.I.

Conflict of interest

None.

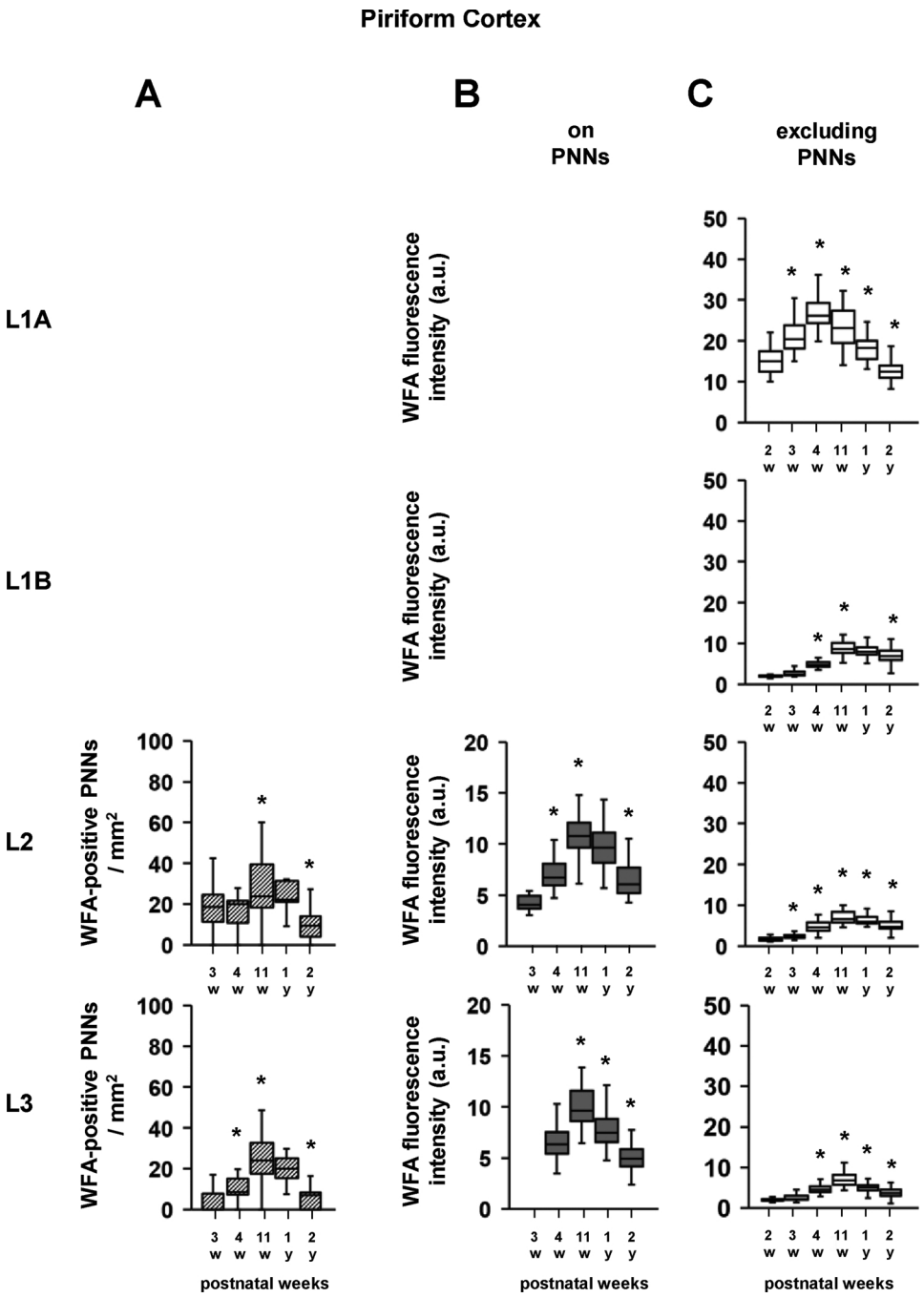

Fig. 10. Quantitative analyses of layer-specific aging patterns of WFA-positive molecules and WFA-positive PNNs in the mouse piriform cortex.
Quantified density of WFA-positive PNNs (A), mean fluorescence intensity of WFA-positive PNNs (B), and mean fluorescence intensity of WFA-positive molecules, excluding the PNN, (C) in L1A, L1B, L2, and L3 of the mouse piriform cortex. Data are expressed as box plots. Statistical significance is represented by asterisks: *$p < 0.05$. Statistically significant differences were compared with earlier age groups. The respective p values are listed in Table 3.
L2: $F_{(4,88)} = 6.688$, $p < 0.001$, L3: $F_{(4,88)} = 17.884$, $p < 0.001$ in.(A). L2: $F_{(4,152)} = 36.563$, $p < 0.001$, L3: $F_{(3,124)} = 37.354$, $p < 0.001$ in.(B). L1A: $F_{(5,320)} = 125.407$, $p < 0.001$, L1B: $F_{(5,320)} = 156$, $p < 0.001$, L2: $F_{(5,320)} = 133.327$, $p < 0.001$, L3: $F_{(5,320)} = 94.051$, $p < 0.001$ in.(C).

Funding sources

This work is supported by a Grant-Aid for Kawasaki University of Medical Welfare Scientific Research Fund.

Acknowledgements

We thank Kawasaki Medical School Central Research Institute for making instruments available to support this study. We would like to thank Editage (www.editage.jp) for English language editing.

References

Asher, R.A., Morgenstern, D.A., Moon, L.D., Fawcett, J.W., 2001. Chondroitin sulphate proteoglycans: inhibitory components of the glial scar. Prog. Brain Res. 132, 611–619.

Bandtlow, C.E., Zimmermann, D.R., 2000. Proteoglycans in the developing brain: new conceptual insights for old proteins. Physiol. Rev. 80, 1267–1290.

Barker, M., Solinski, H.J., Hashimoto, H., Tagoe, T., Pilati, N., Hamann, M., 2012. Acoustic overexposure increases the expression of VGLUT-2 mediated projections from the lateral vestibular nucleus to the dorsal cochlear nucleus. PLoS One 7, e35955.

Bekkers, J.M., Suzuki, N., 2013. Neurons and circuits for odor processing in the piriform cortex. Trends Neurosci. 36, 429–438.

Berardi, N., Pizzorusso, T., Maffei, L., 2004. Extracellular matrix and visual cortical plasticity: freeing the synapse. Neuron 44, 905–908.

Berretta, S., 2012. Extracellular matrix abnormalities in schizophrenia. Neuropharmacology 62, 1584–1597.

Bolós, M., Perea, J.R., Terreros-Roncal, J., Pallas-Bazarra, N., Jurado-Arjona, J., Ávila, J., Llorens-Martín, M., 2018. Absence of microglial CX3CR1 impairs the synaptic integration of adult-born hippocampal granule neurons. Brain Behav. Immun. 68, 76–89.

Bonneh-Barkay, D., Wiley, C.A., 2009. Brain extracellular matrix in neurodegeneration. Brain Pathol. 19, 573–585 Brain Res Brain Res Rev 26:285–294.

Brückner, G., Brauer, K., Härtig, W., Wolff, J.R., Rickmann, M.J., Derouiche, A., Delpech, B., Girard, N., Oertel, W.H., Reichenbach, A., 1993. Perineuronal nets provide a

polyanionic, glia-associated form of microenvironment around certain neurons in many parts of the rat brain. Glia 8, 183–200.
Brückner, G., Hausen, D., Härtig, W., Drlicek, M., Arendt, T., Brauer, K., 1999. Cortical areas abundant in extracellular matrix chondroitin sulphate proteoglycans are less affected by cytoskeletal changes in Alzheimer's disease. Neuroscience 92, 791–805.
Burke, S.N., Barnes, C.A., 2006. Neural plasticity in the ageing brain. Nat. Rev. Neurosci. 7, 30–40.
Carulli, D., Pizzorusso, T., Kwok, J.C., Putignano, E., Poli, A., Forostyak, S., Andrews, M.R., Deepa, S.S., Glant, T.T., Fawcett, J.W., 2010. Animals lacking link protein have attenuated perineuronal nets and persistent plasticity. Brain 133, 2331–2347.
Celio, M.R., Spreafico, R., De Biasi, S., Vitellaro-Zuccarello, L., 1998. Perineuronal nets: past and present. Trends Neurosci. 21, 510–515.
Clavaguera, F., Bolmont, T., Crowther, R.A., Abramowski, D., Frank, S., Probst, A., Fraser, G., Stalder, A.K., Beibel, M., Staufenbiel, M., Jucker, M., Goedert, M., Tolnay, M., 2009. Transmission and spreading of tauopathy in transgenic mouse brain. Nat. Cell Biol. 11, 909–913.
Curran, T., D'Arcangelo, G., 1998. Role of Reelin in the Control of Brain Development.
Davis, M.J., Wu, X., Nurkiewicz, T.R., Kawasaki, J., Gui, P., Hill, M.A., Wilson, E., 2002. Regulation of ion channels by integrins. Cell Biochem. Biophys. 36, 41–66.
de Vivo, L., Landi, S., Panniello, M., Baroncelli, L., Chierzi, S., Mariotti, L., Spolidoro, M., Pizzorusso, T., Maffei, L., Ratto, G.M., 2013. Extracellular matrix inhibits structural and functional plasticity of dendritic spines in the adult visual cortex. Nat. Commun. 4, 1484.
Dino, M.R., Harroch, S., Hockfield, S., Matthews, R.T., 2006. Monoclonal antibody Cat-315 detects a glycoform of receptor protein tyrosine phosphatase beta/phosphacan early in CNS development that localizes to extrasynaptic sites prior to synapse formation. Neuroscience 142, 1055–1069.
Dityatev, A., 2010. Remodeling of extracellular matrix and epileptogenesis. Epilepsia 51 (Suppl. 3), 61–65.
Evers, M.R., Salmen, B., Bukalo, O., Rollenhagen, A., Bösl, M.R., Morellini, F., Bartsch, U., Dityatev, A., Schachner, M., 2002. Impairment of L-type Ca2+ channel-dependent forms of hippocampal synaptic plasticity in mice deficient in the extracellular matrix glycoprotein tenascin-C. J. Neurosci. 22, 7177–7194.
Felleman, D.J., Van Essen, D.C., 1991. Distributed hierarchical processing in the primate cerebral cortex. Cereb. Cortex 1, 1–47.
Frischknecht, R., Heine, M., Perrais, D., Seidenbecher, C.I., Choquet, D., Gundelfinger, E.D., 2009. Brain extracellular matrix affects AMPA receptor lateral mobility and short-term synaptic plasticity. Nat. Neurosci. 12, 897–904.
Frischknecht, R., Gundelfinger, E.D., 2012. The brain's extracellular matrix and its role in synaptic plasticity. Adv. Exp. Med. Biol. 970, 153–171.
Frost, B., Jacks, R.L., Diamond, M.I., 2009. Propagation of tau misfolding from the outside to the inside of a cell. J. Biol. Chem. 284, 12845–12852.
Gaudet, A.D., Popovich, P.G., 2014. Extracellular matrix regulation of inflammation in the healthy and injured spinal cord. Exp. Neurol. 258, 24–34.
Geissler, M., Gottschling, C., Aguado, A., Rauch, U., Wetzel, C.H., Hatt, H., Faissner, A., 2013. Primary hippocampal neurons, which lack four crucial extracellular matrix molecules, display abnormalities of synaptic structure and function and severe deficits in perineuronal net formation. J. Neurosci. 33, 7742–7755.
Giamanco, K.A., Morawski, M., Matthews, R.T., 2010. Perineuronal net formation and structure in aggrecan knockout mice. Neuroscience 170, 1314–1327.
Gogolla, N., Caroni, P., Lüthi, A., Herry, C., 2009. Perineuronal nets protect fear memories from erasure. Science 325, 1258–1261.
Härtig, W., Brauer, K., Brückner, G., 1992. Wisteria floribunda agglutinin-labelled nets surround parvalbumin-containing neurons. Neuroreport 3, 869–872.
Härtig, W., Derouiche, A., Welt, K., Brauer, K., Grosche, J., Mäder, M., Reichenbach, A., Brückner, G., 1999. Cortical neurons immunoreactive for the potassium channel Kv3.1B subunit are predominantly surrounded by perineuronal nets presumed as a buffering system for cations. Brain Res. 842, 15–29.
Hrabetová, S., Masri, D., Tao, L., Xiao, F., Nicholson, C., 2009. Calcium diffusion enhanced after cleavage of negatively charged components of brain extracellular matrix by chondroitinase ABC. J. Physiol. 587, 4029–4049.
Isaacson, J.S., 2010. Odor representations in mammalian cortical circuits. Curr. Opin. Neurobiol. 20, 328–331.
Jäger, C., Lendvai, D., Seeger, G., Brückner, G., Matthews, R.T., Arendt, T., Alpár, A., Morawski, M., 2013. Perineuronal and perisynaptic extracellular matrix in the human spinal cord. Neuroscience 238, 168–184.
Jiao, Y., Zhang, C., Yanagawa, Y., Sun, Q.Q., 2006. Major effects of sensory experiences on the neocortical inhibitory circuits. J. Neurosci. 26, 8691–8701.
John, N., Krügel, H., Frischknecht, R., Smalla, K.H., Schultz, C., Kreutz, M.R., Gundelfinger, E.D., Seidenbecher, C.I., 2006. Brevican-containing perineuronal nets of extracellular matrix in dissociated hippocampal primary cultures. Mol. Cell. Neurosci. 31, 774–784.
Kalb, R.G., Hockfield, S., 1994. Electrical activity in the neuromuscular unit can influence the molecular development of motor neurons. Dev. Biol. 162, 539–548.
Karetko-Sysa, M., Skangiel-Kramska, J., Nowicka, D., 2014. Aging somatosensory cortex displays increased density of WFA-binding perineuronal nets associated with GAD-negative neurons. Neuroscience 277, 734–746.
Kfoury, N., Holmes, B.B., Jiang, H., Holtzman, D.M., Diamond, M.I., 2012. Trans-cellular propagation of Tau aggregation by fibrillar species. J. Biol. Chem. 287, 19440–19451.
Kochlamazashvili, G., Henneberger, C., Bukalo, O., Dvoretskova, E., Senkov, O., Lievens, P.M., Westenbroek, R., Engel, A.K., Catterall, W.A., Rusakov, D.A., Schachner, M., Dityatev, A., 2010. The extracellular matrix molecule hyaluronic acid regulates hippocampal synaptic plasticity by modulating postsynaptic L-type Ca(2+) channels. Neuron 67, 116–128.
Lendvai, D., Morawski, M., Négyessy, L., Gáti, G., Jäger, C., Baksa, G., Glasz, T., Attems, J., Tanila, H., Arendt, T., Harkany, T., Alpár, A., 2013. Neurochemical mapping of the human hippocampus reveals perisynaptic matrix around functional synapses in Alzheimer's disease. Acta Neuropathol. 125, 215–229.
Levy, A.D., Omar, M.H., Koleske, A.J., 2014. Extracellular matrix control of dendritic spine and synapse structure and plasticity in adulthood. Front. Neuroanat. 8, 116.
Li, W., Howard, J.D., Gottfried, J.A., 2010. Disruption of odour quality coding in piriform cortex mediates olfactory deficits in Alzheimer's disease. Brain 133, 2714–2726.
Maeda, N., 2015. Proteoglycans and neuronal migration in the cerebral cortex during development and disease. Front. Neurosci. 9, 98.
Matthews, R.T., Kelly, G.M., Zerillo, C.A., Gray, G., Tiemeyer, M., Hockfield, S., 2002. Aggrecan glycoforms contribute to the molecular heterogeneity of perineuronal nets. J. Neurosci. 22, 7536–7547.
Mauney, S.A., Athanas, K.M., Pantazopoulos, H., Shaskan, N., Passeri, E., Berretta, S., Woo, T.U., 2013. Developmental pattern of perineuronal nets in the human prefrontal cortex and their deficit in schizophrenia. Biol. Psychiatry 74, 427–435.
McKeon, R.J., Schreiber, R.C., Rudge, J.S., Silver, J., 1991. Reduction of neurite outgrowth in a model of glial scarring following CNS injury is correlated with the expression of inhibitory molecules on reactive astrocytes. J. Neurosci. 11, 3398–3411.
McKeon, R.J., Höke, A., Silver, J., 1995. Injury-induced proteoglycans inhibit the potential for laminin-mediated axon growth on astrocytic scars. Exp. Neurol. 136, 32–43.
McRae, P.A., Rocco, M.M., Kelly, G., Brumberg, J.C., Matthews, R.T., 2007. Sensory deprivation alters aggrecan and perineuronal net expression in the mouse barrel cortex. J. Neurosci. 27, 5405–5413.
Mercier, F., Kwon, Y.C., Douet, V., 2012. Hippocampus/amygdala alterations, loss of heparan sulfates, fractones and ventricle wall reduction in adult BTBR T+ tf/J mice, animal model for autism. Neurosci. Lett. 506, 208–213.
Miyata, S., Nishimura, Y., Nakashima, T., 2007. Perineuronal nets protect against amyloid beta-protein neurotoxicity in cultured cortical neurons. Brain Res. 1150, 200–206.
Morawski, M., Brückner, G., Jäger, C., Seeger, G., Arendt, T., 2010. Neurons associated with aggrecan-based perineuronal nets are protected against tau pathology in subcortical regions in Alzheimer's disease. Neuroscience 169, 1347–1363.
Morawski, M., Brückner, M.K., Riederer, P., Brückner, G., Arendt, T., 2004. Perineuronal nets potentially protect against oxidative stress. Exp. Neurol. 188, 309–315.
Morris, N.P., Henderson, Z., 2000. Perineuronal nets ensheath fast spiking, parvalbumin-immunoreactive neurons in the medial septum/diagonal band complex. Eur. J. Neurosci. 12, 828–838.
Mouw, J.K., Ou, G., Weaver, V.M., 2014. Extracellular matrix assembly: a multiscale deconstruction. Nat. Rev. Mol. Cell Biol. 15, 771–785.
Moyer, C.E., Erickson, S.L., Fish, K.N., Thiels, E., Penzes, P., Sweet, R.A., 2016. Developmental trajectories of auditory cortex synaptic structures and gap-prepulse inhibition of acoustic startle between early adolescence and young adulthood in mice. Cereb. Cortex 26, 2115–2126.
Nakagawa, F., Schulte, B.A., Wu, J.Y., Spicer, S.S., 1986. GABAergic neurons of rodent brain correspond partially with those staining for glycoconjugate with terminal N-acetylgalactosamine. J. Neurocytol. 15, 389–396.
Okamoto, M., Mori, S., Endo, H., 1994. A protective action of chondroitin sulfate proteoglycans against neuronal cell death induced by glutamate. Brain Res. 637, 57–67.
Pantazopoulos, H., Woo, T.U., Lim, M.P., Lange, N., Berretta, S., 2010. Extracellular matrix-glial abnormalities in the amygdala and entorhinal cortex of subjects diagnosed with schizophrenia. Arch. Gen. Psychiatry 67, 155–166.
Paxinos, G., Franklin, K.B.J., 2012. Paxinos and Franklin's the Mouse Brain in Stereotaxic Coordinates, 4th ed. Academic Press.
Pitkänen, A., Ndode-Ekane, X.E., Łukasiuk, K., Wilczynski, G.M., Dityatev, A., Walker, M.C., Chabrol, E., Dedeurwaerdere, S., Vazquez, N., Powell, E.M., 2014. Neural ECM and epilepsy. Prog. Brain Res. 214, 229–262.
Pizzorusso, T., Medini, P., Berardi, N., Chierzi, S., Fawcett, J.W., Maffei, L., 2002. Reactivation of ocular dominance plasticity in the adult visual cortex. Science 298, 1248–1251.
Pizzorusso, T., Medini, P., Landi, S., Baldini, S., Berardi, N., Maffei, L., 2006. Structural and functional recovery from early monocular deprivation in adult rats. Proc. Natl. Acad. Sci. U. S. A. 103, 8517–8522.
Risher, W.C., Patel, S., Kim, I.H., Uezu, A., Bhagat, S., Wilton, D.K., Pilaz, L.J., Singh Alvarado, J., Calhan, O.Y., Silver, D.L., Stevens, B., Calakos, N., Soderling, S.H., Eroglu, C., 2014. Astrocytes refine cortical connectivity at dendritic spines. Elife 17, 3.
Sceniak, M.P., Lang, M., Enomoto, A.C., James Howell, C., Hermes, D.J., Katz, D.M., 2016. Mechanisms of functional hypoconnectivity in the medial prefrontal cortex of Mecp2 null mice. Cereb. Cortex 26, 1938–1956.
Schiff, M.L., Reyes, A.D., 2012. Characterization of thalamocortical responses of regular-spiking and fast-spiking neurons of the mouse auditory cortex in vitro and in silico. J. Neurophysiol. 107, 1476–1488.
Schweizer, M., Streit, W.J., Müller, C.M., 1993. Postnatal development and localization of an N-acetylgalactosamine containing glycoconjugate associated with nonpyramidal neurons in cat visual cortex. J. Comp. Neurol. 329, 313–327.
Seeger, G., Brauer, K., Härtig, W., Brückner, G., 1994. Mapping of perineuronal nets in the rat brain stained by colloidal iron hydroxide histochemistry and lectin cytochemistry. Neuroscience 58, 371–388.
Senkov, O., Andjus, P., Radenovic, L., Soriano, E., Dityatev, A., 2014. Neural ECM molecules in synaptic plasticity, learning, and memory. Prog. Brain Res. 214, 53–80.
Silver, J., 1994. Inhibitory molecules in development and regeneration. J. Neurol. 242, 22–24.
Slaker, M., Blacktop, J.M., Sorg, B.A., 2016. Caught in the net: perineuronal nets and addiction. Neural Plast. 2016, 7538208.
Smith-Thomas, L.C., Stevens, J., Fok-Seang, J., Faissner, A., Rogers, J.H., Fawcett, J.W., 1995. Increased axon regeneration in astrocytes grown in the presence of

proteoglycan synthesis inhibitors. J. Cell. Sci. 108, 1307–1315.
Srinivasan, J., Schachner, M., Catterall, W.A., 1998. Interaction of voltage-gated sodium channels with the extracellular matrix molecules tenascin-C and tenascin-R. Proc. Natl. Acad. Sci. U. S. A. 95, 15753–15757.
Strauch, C., Manahan-Vaughan, D., 2018. In the piriform cortex, the primary impetus for information encoding through synaptic plasticity is provided by descending rather than ascending olfactory inputs. Cereb. Cortex 28, 764–776.
Suttkus, A., Rohn, S., Weigel, S., Glöckner, P., Arendt, T., Morawski, M., 2014. Aggrecan, link protein and tenascin-R are essential components of the perineuronal net to protect neurons against iron-induced oxidative stress. Cell Death Dis. 5, e1119.
Suttkus, A., Holzer, M., Morawski, M., Arendt, T., 2016a. The neuronal extracellular matrix restricts distribution and internalization of aggregated Tau-protein. Neuroscience 313, 225–235.
Suttkus, A., Morawski, M., Arendt, T., 2016b. Protective properties of neural extracellular matrix. Mol. Neurobiol. 53, 73–82.
Ueno, H., Suemitsu, S., Okamoto, M., Matsumoto, Y., Ishihara, T., 2017. Sensory experience-dependent formation of perineuronal nets and expression of Cat-315 immunoreactive components in the mouse somatosensory cortex. Neuroscience 355, 161–174.
Ueno, H., Takao, K., Suemitsu, S., Murakami, S., Kitamura, N., Wani, K., Okamoto, M., Aoki, S., Ishihara, T., 2018. Age-dependent and region-specific alteration of parvalbumin neurons and perineuronal nets in the mouse cerebral cortex. Neurochem. Int. 112, 59–70.
Vaughan, D.N., Jackson, G.D., 2014. The piriform cortex and human focal epilepsy. Front. Neurol. 5, 259.
Vogt, B.A., Crino, P.B., Volicer, L., 1991. Laminar alterations in gamma-aminobutyric acidA, muscarinic, and beta adrenoceptors and neuron degeneration in cingulate cortex in Alzheimer's disease. J. Neurochem. 57, 282–290.
Winer, J.A., Miller, L.M., Lee, C.C., Schreiner, C.E., 2005. Auditory thalamocortical transformation: structure and function. Trends Neurosci. 28, 255–263.
Zimmermann, D.R., Dours-Zimmermann, M.T., 2008. Extracellular matrix of the central nervous system: from neglect to challenge. Histochem. Cell Biol. 130, 635–653.
Zuo, J., Neubauer, D., Dyess, K., Ferguson, T.A., Muir, D., 1998. Degradation of chondroitin sulfate proteoglycan enhances the neurite-promoting potential of spinal cord tissue. Exp. Neurol. 154, 654–662.